# Sandwich Construction For Ship Superstructure: Cost Estimation And Failure Prediction

by



A thesis submitted to the

School of Graduate Studies

in partial fulfilment of the

requirements for the degree of

Master of Engineering

in

Mechanical Engineering

Faculty of Applied Science and Engineering

Memorial University of Newfoundland

December 2016

St. John's Newfoundland

## Abstract

The thesis emphasizes on the theoretical and numerical investigations of sandwich structures, especially the web-core sandwich structure. A mathematical model is applied to estimate the manufacturing cost of a glass-fiber reinforced plastic web-core sandwich hatch cover panel using the vacuum assisted resin transfer molding. The advantages of the composite hatch cover panel compared to the convention steel one are illustrated. The buckling of web-core sandwich structure is studied to reveal the effects of webs and core material on the critical buckling loads. The variational iteration method is used and approved to be efficient and accurate as an approximate method. The finite element analysis simulation using Abaqus is conducted to facilitate the research of sandwich wrinkling phenomenon. The sandwich structures with both Aluminum and composites face-sheets are covered in the finite element analysis simulations. The effects of boundary conditions and element types are demonstrated. The finite element analysis results are compared with that of both analytical models and testings, and the disparities are explained.

## Acknowledgements

I would like to express my sincere gratitude to my supervisor Dr. Sam Nakhla for his continuous support during my master studies. His patience, guidance, encouragement and immense knowledge make it possible for me to accomplish my research work.

I also would like to acknowledge all my colleagues for offering their help. Their help made me feel I was not alone when I was stuck in tough problems.

Besides, I would like to acknowledge all the researchers and professors whom I have discussed and consulted questions with. The discussions and consultations really inspired me and solved many problems.

Moreover, I would like to acknowledge Research and Development Corporation Newfoundland and Labrador (RDCNL) for their financial support.

Finally, I would like to acknowledge my families and friends for their support, encouragement and understanding. I can never survive the hard work and stress without them around me.

# Contents

# List of Tables

# List of Figures

# Chapter 1

# Introduction

With the improvement and optimization of manufacturing processes and the decrease of cost, the application of composites material has expanded from military purposes to various engineering areas because of their excellent advantages over conventional metallic material, such as light weight (high strength to weight ratio), tailorable mechanical properties, and good heat, fatigue and corrosion resistance.

The composites material comprises two or more constituent materials to provide a desirable combination of mechanical performance. For glass-fiber reinforced plastic (GFRP) or carbon-fiber reinforced plastic (CFRP), the main components are fibers and matrix. Another widely used type of composites material is the sandwich structure, which consists of two face-sheets and a core. The face-sheets can be GFRP, CFRP, aluminum, and other alloys. The core can be open and closed-cell foams, honeycomb, balsa and cellular lattices. The face-sheets are boned to the core. The sandwich structure provides higher bending stiffness with reduced self-weight. Different sandwich structure types, for instance, web-core sandwich panel and corrugated sand-

wich panel, were developed to satisfy special requirements. The web-core sandwich panel can be used in large ships as hatch covers, deck panels or ship super-structures. However, concerns regarding the manufacturing cost and failure of composites sandwich structures are slowing down the further growth of the composites sandwich application. The demand for research in terms of cost estimation of large composites parts and failure prediction of different sandwich structures is urgent.

## 1.1 Cost estimation techniques

Since the 1970s, significant efforts have been taken by researchers to estimate the manufacturing cost of composites parts. Numerous models and frameworks have been proposed and almost all of them are developed for the manufacturing of aerospace composites parts. Many models rely heavily on practical industry manufacturing data. For the fabrication of the fiber-reinforced plastic (FRP), various fibers and matrix combinations and many fabrication processes can be chosen, which complicates the design and cost estimation. The selection of fabrication process and materials is determined by design and quality requirements. Therefore, numerous cost analysis models and techniques have been established for both design and manufacturing stages. The production cost can be reduced by optimizing the design and choosing suitable fabrication processes. It is worth noting that no models or techniques concerning the cost estimation of web-core sandwich structure are found in the literature.

## 1.2 Sandwich structure failure prediction

The failure modes of sandwich structures include the failure of face-sheets under compressive and extensional loads, face-sheets indentation failure under concentrated loads, core failure, debonding between face-sheets and core, global buckling and wrinkling. The failure modes are related to material properties, structure geometries and the types of load applied. Besides, one failure mode may initiate other failures, which makes the failure modes coupled and intricate. Numerous research was conducted to investigate the failure modes and their interactions, and these research results and theories are then used as design criteria in industries.

Wrinkling is a local buckling phenomenon of sandwich structure under compression loads, Figure 1.1. The wrinkling of sandwich structures has been investigated theoretically, experimentally and numerically. Different theoretical models for both isotropic and anisotropic face-sheets have been proposed and have been verified by experiments or finite element analysis. Those models are based on different assumptions and methods to solve this problem. Therefore, different equations have been derived to predict the critical wrinkling loads. Some of the explicit equations are commonly adopted in industrial designs.

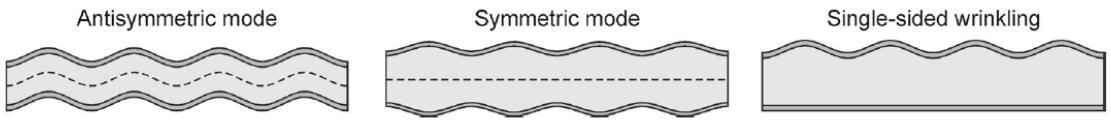


Figure 1.1: Three different wrinkling modes [3]

## 1.3 The application of composites material in ship structures

Nowadays, most large vessels are made of steel. The manufacturing and building technologies are quiet advanced and systematic. Compared with the steel vessel building, the large composites ship structure manufacturing and application are still underdeveloped. The application of composites material will play a significant role in the innovation of ship structures. For instance, the fiber-reinforced plastic (FRP) can provide higher specific strength and stiffness with lower structure weight. Less structure weight is required by warship to increase speed. The reduced structure weight also means more cargo loads and less fuel consumptions for cargo ships and oil tankers. Another unique advantage of fiber-reinforced plastic (FRP) is its non-magnetic property, which is important for surface warships, especially the minesweepers.

The successful applications of composites in marine structures are limited to passenger ferries, fishing and recreational boats and non-structural parts in large steels ships, such as hatch covers of cargo ships, masts of destroyers and funnel on cruise ships. The limitations of the wider application of composites in marine structures are from two aspects: the economic aspect and technical aspect. The economic aspect refers to manufacturing cost and maintenance cost while the technical aspect refers to manufacturing techniques, joining techniques, structure failures and other aspects of the mechanical performance in harsh sea environment. In some design, the priority is given to the structural integrity to reduce joining between parts when a large complex part is fabricated. The consideration of structural integrity and the challenge to assure the quality of the large part complicate the composites manufacturing process.

One of the manufacturing methods that can be used for large ship structures is the vacuum assisted resin transfer molding (VARTM). VARTM is widely employed due to its features of lower cost, room temperature manufacturing environment and ease to scale to different sizes.

## 1.4 Thesis Outlines

As mentioned in the section above, both economic and technical feasibility are essential for the development of composites for large ship structures. The specific manufacturing cost estimation models for composites ship structures are demanded. Besides, the failure modes should be investigated to achieve reliable mechanical performance. The research presented in this thesis emphasizes the feasibility study of large web-core composites sandwich structures, the theoretical modeling of web-core structure buckling and the finite element analysis of regular composites sandwich structures.

Chapter 2 includes the literature review with respect to cost estimation models and the wrinkling failure prediction of sandwich structures, respectively. Various models and methods are compared and discussed.

Chapter 3 presents the feasibility study of web-core sandwich structures composed of GFRP face-sheets and webs and foam core. This sandwich structure has the potential to be used as hatch covers for large cargo ships. The method to estimate the manufacturing cost is proposed and the estimated cost is compared to that of conventional steel structures. The strength and stiffness are also compared between the composites hatch cover and the steel one.

Chapter 4 emphasizes the buckling of web-core sandwich structures. The periodic

unit of the web-core sandwich structure is modeled as column resting on the Pasternak foundation with rotational end constraints. The effects of core and webs on the critical buckling loads are investigated using the variational iteration method.

Chapter 5 illustrates the application of finite element analysis to analyze the sandwich wrinkling phenomenon. The effects of boundary conditions and element types for face-sheets are studied. The finite element models are based on the specimens and testing data documented in the literature. The accuracy and efficiency of the finite element analysis simulation are demonstrated.

Chapter 6 concludes the thesis and suggests future research based on present research results.

# Chapter 2

# Literature Review

## 2.1 The application of sandwich structures in shipbuilding

Numerous research papers regarding the application of composites and sandwich structures to ship building industrial have been published. The design guides for composite ship structures were suggested in [7]. The improvement of materials and building practice were considered in the guides. Mouritz *et al* [8] reviewed the advanced composite structures for naval vessels and their potential applications to submarines. The main benefits and drawbacks of using composite structures were discussed. In the aspects of sandwich structure design, inspection, repair and joining technologies, practice guidelines were provided in [9] for marine application designers and engineers. Kujala and Klanac [10] summarized the application of steel sandwich panels in shipbuilding field. Main benefits and problems as well as related design tools were discussed and a case study was provided as the demonstration. China

Classification Society published guidelines for the application of steel sandwich panel constructions to ship structures [11]. Detailed requirements were outlined for various sandwich structure applications.

## 2.2 Cost estimation

In this section, the cost estimation methods and models are reviewed. The research regarding cost optimization and the effects of uncertainty in cost estimation is discussed.

### 2.2.1 Cost estimation methods for the composites parts manufacturing

In terms of cost analysis techniques and models for composites, Northrop Corporation [12] developed an estimation model for the recurring cost in the Advanced Composite Cost Estimating Manual Program for the manufacturing of advanced composites parts. The recurring cost comprised of indirect and direct cost, and the direct cost was further divided into labor and material cost. The model was valid because it was based on massive industrial data solicited during the program.

Gutowski *et al* [13] developed a general model, called 'first-order dynamic model' to estimate the composites fabrication time. The fundamental idea of the model was to assume that each sub-processes was a first-order dynamic system. The $v_0$, the maximum velocity during the process step, and $\tau$, the dynamic time constant, characterize the process time estimation equation. The two constants were based on the physical characteristics of the different processes and could be adjusted accordingly

for different manufacturing processes. For the parts with complex shapes, the information theory was introduced into the model to describe the complexity. The model was validated by the results in [12].

A systematic framework for estimating the fabrication time of composites parts was established by Neo [14] in his Ph.D dissertation. In the adaptive framework, every process step was matched with an equation and relevant constants were provided. Manufacturing techniques that were widely used in industries, such as hand layup (HLU), automatic tow placement (ATP) and resin transfer molding (RTM) were included in the framework. The cost drivers of different manufacturing technologies were also identified. This framework was verified to be general, robust, easy to be modified and relatively straight-forward. New fabrication processes can also be added to the framework.

Haffner extended the research results of Gutowski and Neo and further provided a more comprehensive framework in [6]. The relatively new manufacturing techniques, i.e. pultrusion and double diaphragm forming (DDF), were covered in his research. Furthermore, the investment cost for equipment and tooling was also considered. The analysis and comparison of the effects of part complexities were elucidated.

Based on the work of Gutowski and Neo [13, 14], Ye *et al* [15] proposed a method to estimate the cost of manufacturing composite waved beams. The total cost was divided into equipment cost, tooling cost, labor cost and material cost. The authors elaborated on the labor cost estimation. The autoclave cure method was used for the fabrication and a detailed process flow was provided. The applicability and accuracy of the model was verified by experiments. The effects of changing the values of model parameters were demonstrated based on their experimental results.

### 2.2.2 Cost optimization of composites products manufacturing

Kassapoglou [16] optimized the structure weight, cost or the combination of both weight and cost taking account of structural requirements and manufacturing constraints. Four different manufacturing methods, i.e. conventional sheet metal, high speed machined metal, hand laid-up composites, and resin transfer molded composites, were compared. The manufacturing process constraints of each method were translated to geometric limitations in design. The results of his research showed that the resin transfer molding (RTM) process was in the lowest cost and weight point when the frames were lightly loaded. However, the RTM yields only the lowest weight design when the frames were highly loaded.

A new approach to optimize both cost and weight of aerospace structures was provided in [17]. The parameter $\Delta\$/\Delta Kg$, which described the money increment required to achieve the increments of weight reduction, was the primary design driver. The methodology was applied to a simplified aileron structure and the Krueger flap. The new approach was compared with the Pareto approach, the standard multi-objective optimization method, to reveal its advantages.

Bernet *et al* [18] proposed a cost estimation model to assess the cost saving potential of a novel composites processing technique. In this model, the total manufacturing cost was divided into material cost, labor cost and overhead cost. Analytically solvable equations were presented for every cost part correspondingly. Furthermore, the processing time of each operation in the labor cost part was divided into the setup time, run time, move time and wait time. The cost model was integrated with a

validated consolidation model; therefore, the manufacturing cost depended on the required part quality and vice versa, because the cost, processing parameters and part quality were coupled. The model was successfully used to investigate the production of generic hooks.

A framework to minimize the direct operating cost (DOC) was developed in [19]. The non-destructive test cost was implemented into the framework as a part of the DOC. The weighted sum of manufacturing cost, non-destructive in-production testing cost, single in-service inspection cost and structure weight were included to develop the objective function. A case study was carried out using a generic skin/stinger element. It was found that the design and quality level of the laminates had direct influence on manufacturing cost, testing cost and the structure weight.

### 2.2.3 Cost estimation with uncertainties

In practice, many decisions concerning cost need to be made even when future situations are not certain. In terms of production cost models with uncertainties, Jha [20] developed a mathematical model based on the stochastic geometric program to predict the range of production cost. The exact cost can also be determined using a two stage stochastic geometric program when required. The model can help managers make economic decisions in advance of the production.

For the cost estimation of flat plate processes, Jahan-Shahi *et al* [21] employed a fuzzy set and probability distribution to tackle the uncertainties from imprecise or subjective criteria and random factors. The investigation was conducted within the Activity-Based Costing framework and a simple fuzzy approach was used. The

method was shown to be flexible and reliable. An intelligent knowledge-based product cost estimation system for early design stage was developed by Shehab and Abdalla [22]. A fuzzy logic approach was implemented to guarantee the reliability of the estimation. The system can be used to estimate the cost of material, mould and processing. A case study was presented to validate the estimation system.

The stochastic nature in the shop floor production environment was also considered in the model presented in [23]. The integration of simulation results and optimization were used as two main parts of the model. The estimation of the marginal cost of new orders were enabled. The increase of effectiveness and efficiency of the model were achieved.

## 2.3 Failure prediction of sandwich structures

As mentioned in section 1.2, failure modes of sandwich structure are complex and coupled. The failure model emphasized in this paper is buckling and wrinkling phenomenon. The previous research regarding sandwich buckling and wrinkling is divided into theoretical modeling, testing and finite element modeling and are reviewed.

### 2.3.1 Theoretical molding

The wrinkling of sandwich structure was investigated in [24]. In the paper, eight cases of the face-sheets and supporting medium combinations were studies theoretically. In these combinations, the core thickness was assumed to be either finite or semi-infinite. Another five assumptions were made, which include (1) the compression was all carried by the skin, (2) the continuous supporting medium could be extended

or compressed, (3) the longitudinal forces acting on the surface of the medium were neglected when the skin thickness and deflection amplitudes were small compared with wavelengths, (4) longitudinal movement of the surface of the medium was neglected for the complete skin-medium adhesion situations and (5) no shear stress between skin and medium for the non-adhesion situations. Four of the eight cases were tested. Satisfactory agreements between theoretical and testing results were found.

Hoff and Mautner [25] presented buckling formulas for both symmetric and anti-symmetric shapes based on the theory of minimum total potential energy. To make the model more practical and accurate, the margin zone, which was the part of the core affected by face wrinkling, was introduced in the derivation of the buckling formulas. The formulas of the model ($\nu_c = 0.3$) are shown as follows:

$$\sigma_{cr} = 0.91\sqrt[3]{E_f E_c G_c}, \text{ for symmetric wrinkling of thick sandwich} \tag{2.1a}$$

$$\sigma_{cr} = 0.577\sqrt[3]{E_f E_c \frac{t_f}{t_c}} + 0.33 G_c \frac{t_c}{t_f}, \text{ for symmetric wrinkling of thin sandwich} \tag{2.1b}$$

$$\sigma_{cr} = 0.51\sqrt[3]{E_f E_c G_c} + 0.66 G_c \frac{t_c}{t_f}, \text{ for antisymmetric wrinkling of thick sandwich} \tag{2.1c}$$

$$\sigma_{cr} = 0.417\sqrt[3]{E_f E_c \frac{t_f}{t_c}} + 0.773 G_c \frac{t_c}{t_f}, \text{ for antisymmetric wrinkling of thin sandwich} \tag{2.1d}$$

where $\sigma_{cr}$ is the critical stress, $E_f$ and $t_f$ is the elastic modulus and thickness of the face-sheet, and $E_c$, $G_c$ and $t_c$ is the elastic modulus, shear modulus and thickness of the core, respectively. Besides, the symmetric wrinkling situation was also solved using the elasticity theory [26]. Fifty-one specimens were tested and the results were

compared with the theoretical values, and reasonable agreements were found.

Nardo [27] derived the exact solutions for the buckling of sandwich panel with loaded edges clamped and unloaded edges simply supported. The problem was solved in the elastic range. Shear deformation was included in the equations of equilibrium. Numerical results were obtained and the effects of plate aspect ratio and the ratio of core thickness to plate thickness were investigated.

The report [28] summarized the previous research results before 1961 and reaffirmed the results with experiments. The whole report was divided into three parts including mathematic analysis, comparison between experimental results and theoretical analysis, and the design criteria. The method presented in [24] was first reviewed and related formulas were derived. Then, more complicated assumptions were used, therefore, more sophisticated critical stress formulas were obtained. The irregularities of face sheets, which lower the critical wrinkling stresses, were considered in the mathematical analysis. Four different failure modes which were possible to occur, were tested in the second part of the report. Materials, specimen configurations, test methods and testing results were documented in details. The testing results were compared to corresponding theoretical ones and reasonable agreements were found in the plots. Finally, design criteria and suggestion were given in the last part of the report.

In Plantema's model [29], an exponential decay of the core displacements in the thickness direction of the sandwich structure was assumed, Equation 2.2:

$$w_c = w_f \, e^{-kz} = W e^{-kz} \sin \frac{n\pi x}{l} \tag{2.2}$$

where $W$ is the wave amplitude, $l$ is the length of the sandwich structure, $n$ is the

number of half waves and $k$ is the constant describing the exponential decay of displacement. The subscripts $c$ and $f$ indicate the face-sheet and core. The assumption implies that only transverse deformation was considered and the longitudinal deformation was ignored. The theory of minimum total potential energy was also implemented in his model. Plantema's model assumed that the core was infinitely thick and was valid for infinitely long plate. The critical wrinkling stress for the case of $\nu_c = 0.3$ was obtained as

$$\sigma_{cr} = 0.85\sqrt[3]{E_f E_c G_c} \tag{2.3}$$

Despite the theories above, the general solution unifying global buckling and wrinkling is another approach, where global buckling is considered as a special case of wrinkling. Banson and Mayers [30] presented a unified model to investigate global buckling and wrinkling of sandwich column and plate simultaneously. In their model, the sandwich structure was consisted of isotropic faces and orthotropic core. The variational method was applied in the development of the model. Two cases, namely, buckling analysis (anti-symmetric modes) of simply supported plates and column, and buckling analysis (anti-symmetric and symmetric modes) of the plate with clamped loaded edges and fully supported core, were studied. For both cases, the term stability boundary, which separated general instability and face wrinkling (both symmetric and anti-symmetric) was used, and the boundaries were plotted. The stability boundary can be used as reference for sandwich structure designers. The unified buckling theory for column with simply supported boundaries was compared with existing theories, namely Euler theory, Timoshenko theory and the theory presented in [28]. For the plate with clamped-clamped boundary conditions, the Rayleigh-Ritz method

was applied to derive the approximate expression. The approximation was further compared with the results in [27] for validation.

Allen's model [31] had the same geometric assumptions as that of Plantema. The critical stress was derived by solving the governing equations with the assumption that the core stress field satisfied the Airys stress function. The explicit expression of the model is

$$\sigma_{cr} = B_1 \sqrt[3]{E_f {E_c}^2} \tag{2.4a}$$

$$B_1 = 3[12(3-\nu_c)^2(1+\nu_c)^2]^{-\frac{1}{3}} \tag{2.4b}$$

The critical stress for in-phase buckling based on anti-plane model was also presented by Allen. The formula for the model is as following

$$\sigma_{cr} = \frac{(t_f + t_c)^2 G_c}{2 t_f t_c} \tag{2.5}$$

Theoretical, numerical and experimental investigations of the face-sheet wrinkling of sandwich shell subjected to uniaxial and biaxial compression were conducted by Stiftinger and Rammerstorfer [32]. The critical wrinkling load of orthotropic face-sheets was presented. The term, equivalent stiffness of core which was a parameter of the critical load expression, was proposed and its expression was derived. The effect of the orthotropy of face-sheets and core were investigated. It was concluded that anti-symmetric wrinkling was critical for face sheet with isotropic core and symmetric wrinkling was possible for face sheet with orthotropic core. The numerical results were different from analytical ones for the combined loading condition, especially for thin core structure, while good agreements were shown for thick core sandwich structure. Besides, the effects of material properties (linear elastic face-sheets and linear elastic

core, elastic-plastic face-sheets and linear elastic core, linear elastic face-sheets and crushable core) on the post-buckling behavior were illustrated. Finally, specimens consisted of high strength aluminum alloy face sheet and thick foam core were tested to validate the analytical results. The experimental results were all lower than the analytical results represented by the authors and higher than the results from the expressions of Hoff and Mautner.

Niu and Talreja [33] presented a unified model to incorporate symmetric wrinkling and anti-symmetric wrinkling. In their model, long and short wavelength was defined by the ratio of wrinkling wavelength to core thickness. According to the authors, the long wavelength wrinkling model was only valid for small ratios of core thickness to face-sheet thickness. The Winkler model was modified and the two parameter Pasternak model was evaluated in their paper. The critical stresses are shown below.

$$\sigma_{cr} = \sqrt{\frac{t_f E_c E_f}{3t_c(1-{\nu_c}^2)}} + \frac{(t_c+t_f)^2 E_c}{8t_f t_c(1+\nu_c)} + \frac{(t_c-2t_f\nu_c)E_c}{4t_f(1-\nu_c^2)} \qquad (\frac{\pi t_c}{l_0} \leqslant 1) \tag{2.6}$$

$$\begin{aligned}\sigma_{cr} =& (\frac{3E_c}{2(1+\nu_c)(3-\nu_c)})^{\frac{2}{3}} E_f^{\frac{1}{3}} + \frac{(1-\nu_c)E_c}{(1+\nu_c)(3-\nu_c)} \\ &+ (\frac{E_c}{2(1+\nu_c)(3-\nu_c)})^{\frac{4}{3}} (\frac{3E_f}{2})^{\frac{1}{3}}\end{aligned} \qquad (\frac{\pi t_c}{l_0} \geqslant 1) \tag{2.7}$$

Hadi and Matthews [34] extended the unified model to sandwich column and plate consisted of anisotropic face-sheets and orthotropic core. The effect of adhesive layer was considered in their model. The unified model for sandwich column was compared with the analytical and existing experimental results. Discrepancies were found between the results of this model and Hoff's, Plantema's and Allen's models. The sandwich plate model was validated by the results in the literature for both wrinkling and global buckling phenomenon. Besides, the effect of lamina layup of composites

face-sheet was investigated and the stacking sequence which yielded maximum overall buckling load was found.

Ji and Waas [35] investigated the global and local buckling of a sandwich beam using the classical elasticity theory. The sandwich beam was modeled as the 2D linear elastic continuum. In the derivation of theoretical formulas, general equations of equilibrium for a solid slightly deformed from an initial stress state have been incorporated. Finite element analysis using Abaqus was used then to validate the accuracy of their model. Linear elastic materials were assumed and eight-noded quadratic plane strain elements were used for the face-sheets. The FEA results were compared with the presented analytical results and previous theoretical and testing results. It was found that Niu and Talreja's model yields much lower critical local stresses when stiffer core is used. The authors concluded that anti-symmetric buckling was always dominant rather than symmetric buckling and the theoretical model was applicable to a wide range of material and geometries.

Winkler's elastic foundation approach was also used in the wrinkling prediction of sandwich structures, as explained in [36]. The core was modeled as elastic spring and the critical stress was derived by solving the governing differential equation. The interaction between the elastic springs, i.e. the effect of shear, was ignored in the approach. The drawback of the approach is that it cannot be used in anti-symmetric wrinkling and is not accurate for the thick core, which were also discussed in [33].

### 2.3.2 Sandwich structure wrinkling failure testing

Experimental investigations on wrinkling of sandwich column and plate were documented in [37] and [38]. Both global buckling and wrinkling loads were determined in [37] for sandwich panel with carbon fiber reinforced plastic (CFRP ) face-sheets and honeycomb core. Large disparities were found between testing and theoretical results in [37] so that, as a deeper exploration and discussion, testings were carried out to sandwich columns with CFRP face-sheets in [38]. Better agreements were found in the latter and reasons for the improvement were explained.

Fleck and Sridhar [39] conducted experiments to investigate the failure mode of sandwich columns comprising GFRP face-sheets and PVC foam core under end compression. Euler macro-buckling, core shear macro-buckling, face sheet micro-buckling and face sheet wrinkling were selected as possible failure modes. For the face-sheet wrinkling failure, a modified Hoff's model (the coefficient was reduced to 0.5) was used as theoretical solutions. The collapse mechanism maps were constructed and weight optimization design was conducted according to the research results. It is worth to note that face-sheet wrinkling was not found in the testings for the specimens used in their research.

The wrinkling failure of sandwich column and beam was investigated in [40]. The sandwich beam consisted of unidirectional carbon/epoxy face-sheets and PVC or honeycomb core. The stress-strain relations of the specimens were tested and presented first. Then, the failures of specimens subjected to compression, three- and four- points bending and end load (for cantilever beam) were investigated by testings. The testing results were mainly compared with the research results of Hoff

and Mautner. It was found Hoff and Mautner's model was valid for long beam spans. For short beam spans, core failure may occur first. When the core was degraded, Hoff and Mautner's model was suggested to be modified to take the core degradation effects into account. The results also indicated that the wrinkling stress was dependent of geometrical configurations, which were not included in model of Hoff and Mautner.

### 2.3.3 Wrinkling validation with finite element analysis (FEA)

Vonach and Rammerstorfer [41] presented an analytical model for wrinkling of thick orthotropic sandwich plates on a transversely isotropic thick core. One of the novelties of this work was the application of general load conditions. The limitation of the model was the assumption of a thick core. Due to the lack of existing literature regarding similar research, the 3D FEA simulation in ABAQUS was implemented to validate the theoretical model. The core and face-sheets were modeled with solid and shell elements, respectively. Two sets of periodic boundary conditions were used to fulfill the periodicity nature of wrinkling failure.

Hadi [42] used finite element analysis to model sandwich column wrinkling and compared FEA results with the existing analytical and testing results in [34, 37, 38]. In the FEA model, the face sheet was modeled by the 4 nodes quadrilateral element based on Mindlin-Reisser shell formulation. The FEA simulation was executed within the computer program UNA52. The mode shape was set up to 100 in order to achieve the short wavelength requirement of wrinkling.

Fagerberg and Zenkert [43] investigated the reason of discrepancies between testing and theoretical results found in [2]. They presented an imperfection induced

wrinkling model, which included imperfections of the sinusoidal shape. The in-plane compression strain and bending strain were both affected by the imperfections. As a result, the model gave a relatively conservative prediction of panel strength compared to traditional solutions. The imperfection induced model was proved to be more reasonable and accurate based on their experimental results. The accuracy of the theoretical model was validated by finite element simulation. The plane stress 2D FEA simulation was conducted in ABAQUS. Quadratic beam and membrane elements were used to model face-sheets and core, respectively. Periodic boundary conditions were implemented as [41]. It was concluded the model could be used to select proper core materials to facilitate the sandwich structure design.

## 2.4 Conclusion remarks

The fabrication cost estimation and optimization of composites part have been a popular topic. The focus of existing models and methods is advanced aerospace parts and the research on marine composites structure is relatively limited. The cost estimation research for the large marine composites structure fabrication with the application of specific manufacturing methods, for instance, the vacuum assisted resin transfer molding, is demanded.

Since the 1940s, various methods have been used to investigate the wrinkling of sandwich structure theoretically and numerically. Some theoretical models are simple close-form formula while others may be complex. Due to different assumptions and methods applied, the theories predict the sandwich wrinkling loads discrepantly. Some testings have been conducted to valid theoretical models. In some research, the

testing results only match the theoretical predictions satisfactorily. To eliminate the confusions, the analytical wrinkling models, FEA simulations and testings deserve being studied comprehensively.

# Chapter 3

# REVISITING THE FEASIBILITY STUDY OF COMPOSITES FOR CARGO SHIPS

***Peng Yu, Sam Nakhla***

Faculty of Engineering and Applied Science

Memorial University of Newfoundland

St. John's, Newfoundland, Canada

**Keywords:** feasibility study, composites, cargo ship.

***Abstract:*** *Nowadays, various kinds of composites have been applied by the marine industry, especially in naval vessels and recreational boats. However, the use of composites in cargo ship is still limited and the feasibility study of glass reinforced plastic cargo ship doubted the application of composites for large cargo ships. Considering the*

*development of composites manufacturing and design as well as the improvement of composites properties, this paper revisits the feasibility study of composites for cargo ships and investigates the effects of optimal design of composites on its cost effectiveness. For example, the GRP hatch cover design used in [4] when analyzed is proved to have higher strength and stiffness than the corresponding steel one. Therefore, beyond the weight saving attained using GRP, better structural aspects are accomplished. Hence, the feasibility study on comparing GRP and steel covers is not accurate. The current work is revisiting feasibility study of composite for cargo ships on basis of comparing equivalent structure in terms of strength and stiffness.*

A version of this paper has been published in the *CANCOM2015 - CANADIAN INTERNATIONAL CONFERENCE ON COMPOSITE MATERIALS*. The lead author is Peng Yu and the co-authors is Dr. Sam Nakhla. Mr. Yu's contribution to this paper is as follows:

- Wrote the paper.
- Suggested manufacturing method and process steps in detail.
- Applied the existing cost estimation model to the present structure.
- Conducted the finite element analysis.
- Analyzed the results.

Dr. Nakhla initiated the research idea, provided technical guidance and editing of the manuscript. In this chapter the manuscript is presented with altered figure numbers, table numbers and reference formats in order to match the thesis formatting guidelines set out by Memorial University.

## 3.1 Introduction

Composites have been widely applied by marine industries, such as in naval vessels, small commercial crafts, leisure yachts, sport boats and offshore applications, because of its high specific strength and excellent corrosion resistance. Glass fiber reinforced plastics (GFRP) is relatively cheap among composite materials, which makes it most common in marine industries. The study [4] conducted in 1971 investigated the feasibility of building large GFRP cargo vessels, container ships, bulk carriers and their large structure components technically and economically. It is available in public domain and is widely accepted by ship manufacturers.

Among large structure components, typical hatch cover sections, Figure 3.1, are investigated as a sample in terms of design criteria, weights and construction cost. The steel hatch cover consists of side girders and stiffeners while the composites hatch cover is a web-core sandwich structure. The design of composites cover is based on converting steel thickness to composite thickness and using the ratio between their strength values. Hand layup of pre-preg is assumed as the manufacturing method. The construction cost of the composites structure is $290,000, which is $20,000 higher than that of the corresponding steel one. However, several concerns exist when considering the study in [4], namely (1) composites underwent many advances over the past forty years, especially in introducing new and enhanced resin technologies, (2) manufacturing method, such as vacuum-assisted resin transfer molding (VARTM), is suitable for manufacturing the hatch cover, resulting in higher strength quality without corresponding increase in cost [44, 45, 46], (3) the itemized cost analysis in the study lacks essential detail on materials cost and labor cost, (4) no rigorous de-

sign method is followed or clearly identified in the study, instead, simply converting thickness based on ratio of moduli.

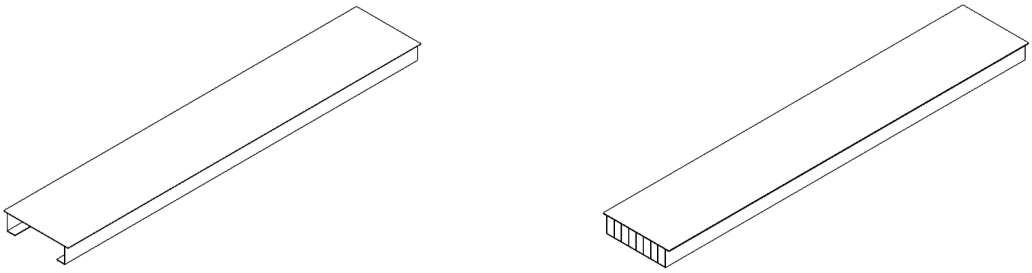

(a) steel hatch cover illustration (b) Composites hatch cover illustration

Figure 3.1: Comparison of steel and composites hatch cover [4]

Due to these concerns, the authors found it necessary to revisit the feasibility study by considering the hatch cover as a sample structure with a major focus on manufacturing and cost. The manufacturing time is estimated using the model and framework presented in [6, 14]. The total construction time is then regenerated and compared with the one presented in [4]. Moreover, composites and corresponding steel structures are compared in terms of strength and stiffness to reveal further aspects and potential of optimizing the cost and structure.

## 3.2 Literature Review on Cost Estimation

Due to limited application of composites to large commercial ships, no cost estimation model or framework specially aiming at large marine composites has been established. In contrast, significant efforts have been made to estimating and optimizing produc-

tion cost in aerospace industries in the last decades. Numerous techniques and models have been developed, many of them could be referred to by marine industries and even be modified to be applicable in marine composites.

Northrop Corporation developed a method [12], Advanced Composite Cost Estimating Manual (ACCEM), to estimate the recurring cost of composites fabrication. In [12], the fabrication time is calculated by summing up the labor time of all steps involved in the manufacturing process. The labor time of every step is estimated using equations of production time based on the best-fit curves of historical cost data from the U.S. government and industries. It is the first systematic methodology for estimating manufacturing cost of composites and has been widely accepted by industries. Gutowski et al developed a theoretical cost model for the composite fabrication [13]. In this model, all sub-process steps are considered to be the first-order system. The first-order dynamic models successfully explained the physical nature of manufacturing processes. Moreover, information theories are incorporated in their model to describe and handle part complexities. Fabrication time from the estimation model shows great consistencies with actual data and those from ACCEM. This model is general and has been verified by hand layup experiments. Based on Gutowskis first-order dynamics model and other existing research results, Neo [14] established a systematic framework for estimating the fabrication time of composites parts in his dissertation. This framework is general, robust, easy to be modified and relatively simple. In the adaptive framework, every process step is matched with an equation and relevant constants are provided. The framework covers hand layup (HLU), automatic tow placement (ATP) and resin transfer molding (RTM).When new fabrication processes occur, they can be added to the framework. Cost drivers of

different manufacturing technologies are also identified. Several years later, Haffner summarized the research of Gutowski and Neo and further provided a comprehensive analysis of cost [6]. His research includes all the common production technologies, namely HLU, ATP, RTM, pultrusion and double diaphragm forming (DDF). It also considers investment cost for equipment and tooling. The analysis and comparison of the effects of part complexities are elaborate in his research. Their research results regarding HLU and RTM are applicable to marine composites.

## 3.3 Cost Estimation of the Hatch Cover

### 3.3.1 Manufacturing method

The US Army has investigated the application of Seeman Composites Resin Infusion Molding Process (SCRIMP$^{TM}$) process to monocoque, single skin stiffened and sandwich configurations in 1994, and the results revealed that the mechanical properties of these structures are satisfying with a relative low cost [44]. Nquyen *et al* [45] in the US Navy evaluated four different low cost manufacturing processes: a vacuum assisted resin transfer molding using ultra-violet resin system, a no-vacuum bag consolidation prepreg system using ultra-violet resin system, a no-vacuum bag without autoclave consolidation of low temperature/energy prepreg system and a patented vacuum assisted resin infusion process known as SCRIMP$^{TM}$. The results demonstrate that a structure manufactured by VARTM is of exceptional quality and the associated cost per pound for manufacturing is lower than the average cost among all four methods. Hence the current study is adopting VARTM as a cost effective

manufacturing method for ship superstructures.

Reference [4] proposed manufacturing a composites hatch cover of a multiple cell sandwich structure, shown in Figure 3.2, to replace the steel one. The multiple cells sandwich panel consists of two face sheets, webs and cores. Top and bottom face sheets and webs are GFRP and eight cores are foam. The dimensions of the composites hatch cover are determined based on the steel one. The specific manufacturing method and cost estimation method of the GFRP hatch cover are not provided.

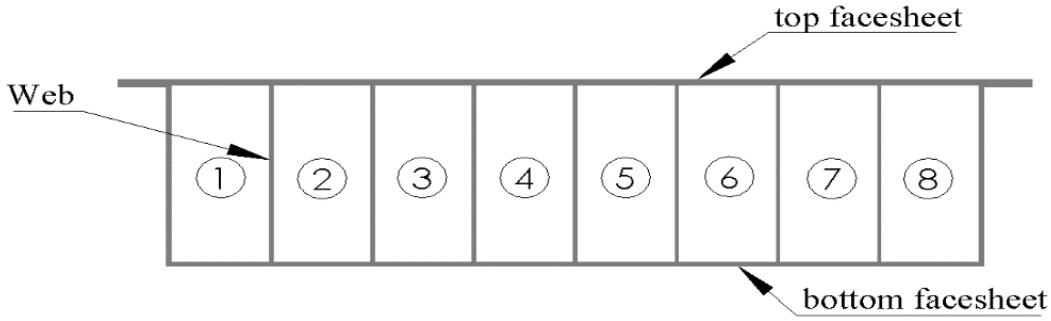


Figure 3.2: Cross section illustration of the hatch cover

### 3.3.2 Manufacturing process

The manufacturing process of a foam-filled web core sandwich panel using VARTM could be summarized as follows: mold preparation, hand lay-up dry fabrics, vacuum bagging and application, resin infusion and curing, demolding and post curing. Two specific approaches are available to manufacture the structure in Figure 3.2. One is to use a "U" shape mold and the fiberglass fabrics are stacked in the order of "bottom face sheetcoretop face sheet"; the other is to use a flat mold and the fiberglass fabrics

are stacked in the order of "top face sheetcorebottom face sheet", as is illustrated in Figure 3.3. Comparing two methods, it is obvious that the "top face sheetcorebottom face sheet" order provides cost saving by utilizing a simpler mold and simpler process.

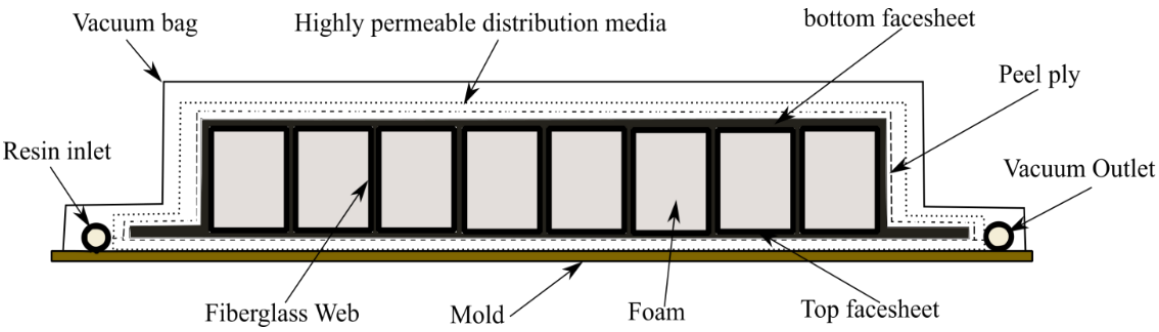


Figure 3.3: Illustration of manufacturing setups

The core design configuration is illustrated in Figure 3.4 [5]. The rectangular foam bars are wrapped by fiberglass fabrics. The core can be fabricated by either hand layup or automated winding process. The top face sheet and bottom face sheet are fabricated by laying up fiberglass fabric above and below the core beams. The fabrication time cost presented in this section is associated to hand layup manufacturing of the core.

### 3.3.3 Labor time estimation

Labor cost is a significant part of over-all manufacturing cost and it is directly related to the labor time. As mentioned earlier, the labor time of manufacturing the composite hatch cover is not provided in details. Therefore, the labor time is estimated in this section.

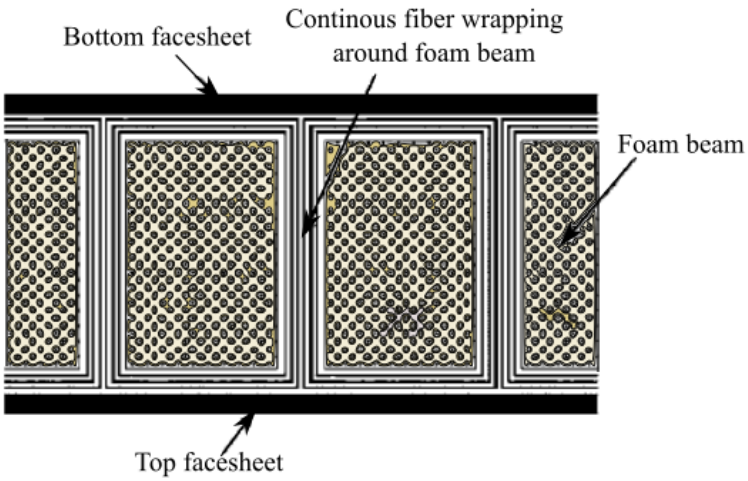


Figure 3.4: Illustration of core design [5]

#### 3.3.3.1 Hand layup time estimation

Hand layup is one of the most time-consuming procedures. Meanwhile, it represents the only valid option when no mass production is intended and hence automation represents an unnecessary added cost. The hand layup procedure includes laying up flat fabric on the mold, wrapping core foam beams with glass fiber fabric, and finally laying up fabric over foam beams. To estimate time related to these steps, a model is presented based on research results in [6, 14].

Based on the first order dynamics model presented by MIT, Gerry Mabson of Boeing Commercial Aircraft Group developed the hyperbolic cost model shown in Equation 3.1 [6, 14],

$$t = \tau_0 \sqrt{(\frac{A}{v_0 \tau_0} + 1)^2 - 1} \tag{3.1}$$

where $t$ is the layup time in minute for laying one layer of fiberglass fabric for flat panels, $\tau_0$ is the dynamic system time constant, $v_0$ is the steady-state velocity constant

and $A$ is the area in square meter of the flat part. The flat panel is shown in Figure 3.5a. The constant $\tau_0$ and $v_0$ are determined by curve fitting the hyperbolic model to ACCEM [12] benchmarks.

When taking the part complexity into consideration, the dynamic system time constant, steady-state velocity constant or both need to be modified to reflect the complexity. According to Haffners work [6], it is reasonable and accurate to modify $\tau_0$ and keep $v_0$ unchanged if the curvature is $\pi/2$, i.e. 90°. The modified dynamic time constant $\tau$ can be expressed as follows,

$$\tau = \tau_0 + b_n I \tag{3.2}$$

$$I = \Delta\Theta L_y \tag{3.3}$$

where $b_n$ is a constant from empirical data, $I$ is to represent the effect of curvature, $\Delta\Theta$ is the angle change in radians compared to flat panel and $L_y$ is the length of the bend, as shown in Figure 3.5b. Accordingly, Equation 3.1 can be modified to estimate the time required for wrapping one layer of fabric over the core material as

$$t_{beam} = (\tau_0 + 4b_n\Delta\Theta L_y)\sqrt{(\frac{A}{v_0(\tau_0 + 4b_n\Delta\Theta L_y)} + 1)^2 - 1} \tag{3.4}$$

The above model is initially established based on pre-preg. In this research, the easiness of laying up pre-preg and dry fabric is assumed to be the same. After incorporating the adaptive framework, the time for wrapping the cores with fiberglass fabric can be estimated using Equation 3.5,

$$T_{beam} = t_{setup} + N_1(t_{delay} + n_1 t_{beam}) \tag{3.5}$$

where $t_{setup}$ represents the time to set up equipment and to prepare for operations, $t_{delay}$ represents the delay time between successive parts after the equipment has been

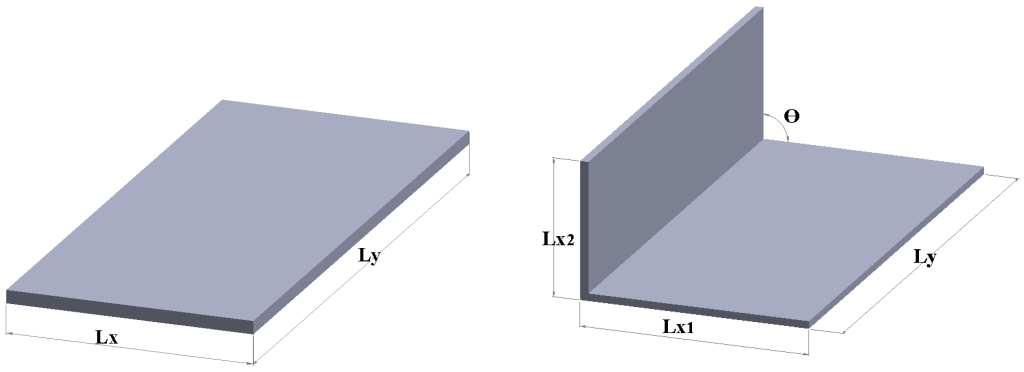


(a) Flat part illustration (b) Part with curvature illustration

Figure 3.5: Illustration of flat and curve part [6]

setup, $N_1$ is the number of core beams and $n_1$ is the number of layers wrapping the core.

The layup time for one layer of fabric of the bottom sheet, $t_{bottom}$, could be estimated by Equation 3.4 and the total time for the bottom sheet could be estimated by Equation 3.6,

$$T_{bottom} = t_{setup} + t_{delay} + n_2 t_{bottom} \tag{3.6}$$

where $n_2$ is the number of fabric layers of the bottom face sheet.

The layup time for one layer of fabric of the top sheet, $t_{top}$, could also be estimated by Equation 3.1 and the total time for the bottom sheet could be estimated using Equation 3.7,

$$T_{top} = t_{setup} + t_{delay} + n_3 t_{top} \tag{3.7}$$

where $n_3$ is the number of layers of the top face sheet.

#### 3.3.3.2 Resin infusion time estimation

Resin infusion significantly affects the time cost and part quality. The resin infusion process of VARTM has been analyzed and modeled in many literature [47, 48, 49, 50, 51]. The resin infusion time for manufacturing the composites hatch cover is estimated based on combining the models presented in [50, 51]. The idea of this model is to estimate VARTM resin infiltration based on the RTM resin filling time considering the use of highly permeable media. According to Darcys law, the resin fill time of resin transfer molding can be obtained by Equation 3.8, which is

$$T_{RTM} = \frac{L^2 * \Phi\mu}{2pK} \tag{3.8}$$

$$K = k\frac{(1 - V_f)^3}{{V_f}^2} \tag{3.9}$$

$$\Phi = 1 - V_f \tag{3.10}$$

where the resin infusion time of RTM is determined by part length $L$, preform permeability $K$, and porosity $\Phi$, resin viscosity $\mu$ and injection pressure $p$. The permeability parameter $K$ is determined by Equation 3.9, where $k$ is the Kozeny coefficient and $V_f$ is the fiber volume fraction, and the porosity of a fiber preform is defined by Equation 3.10. The permeability and porosity have interactions; however, the coupling is not considered in the present work to simplify the model as proposed in [47]. The filling of VARTM is related to that of RTM by the VARTM-RTM mold infusion time ratio $t^*$, which comes from the response surface method. When the fiberglass preform, highly permeable media, resin and injection pressure are determined, the resin infusion time of VARTM can be estimated using Equation 3.11:

$$T_{VARTM} = t^* T_{RTM} \tag{3.11a}$$

$$t^* = \frac{1}{a_0 + a_1 h^* + a_2 K^* + a_{11} h^{*2} + a_{12} h^* K^*} \tag{3.11b}$$

$$K^* = \frac{K_H}{K_f} \tag{3.11c}$$

$$h^* = \frac{h_H}{h_f} \tag{3.11d}$$

The coefficients $a_0$, $a_1$, $a_2$, $a_{11}$ and $a_{12}$ are all from experiment. $h^*$ and $K^*$ are dimensionless variables of thickness and permeability. The subscripts $H$ and $f$ stand for the highly permeable media and fiber preform.

To reduce the resin infusion time and make sure all the fiberglass preforms are wetted out, highly permeable medias are used in both top face sheet and bottom face sheet. Resin injection lines are positioned along the longitudinal direction of the hatch cover, as shown in Figure 3.3. The fill time is estimated by the time that flow front takes to reach the vacuum line end. Parameters needed for fill time estimation is provided in Table 3.1.

#### 3.3.3.3 Time estimation of all steps

Labor time of other procedures, except hand layup and resin infusion, is all estimated using the adaptive framework [14]. The whole manufacturing process procedures needed to fabricate the sandwich hatch cover are listed in Table 3.2. Considering the limitation imposed by the width of fiberglass fabric and the feasibility of practical operations, the width of fiberglass fabric used is one meter and the foam is cut into one-meter-long unit. The length of the hatch cover is 7.85 meters, so one long beam

Table 3.1: Filling time estimation parameters

| Parameters | Values |
|---|---|
| Length | 2.2 (m) |
| Porosity | 0.45 |
| viscosity | 0.23 (Pa s) |
| Injection pressure | $100 \times 10^3$ |
| Kozeny coefficient | $71.8 \times 10^{-12}$ [47] |
| Fiber volume fraction | 0.55 |
| Thickness of HPM | 1 [51] |
| Permeability of Fiberglass perform | $21.6 \times 10^{-12}$ |
| Permeability of HPM | $1.08 \times^{-9}$ |

consists of 8 units (the extra length will be cut off after the whole structure is manufactured). After the foam units are wrapped by fiberglass fabric, they are positioned to the mold. The resin rejection lines are aligned along the length direction to reduce resin fill and vacuum time. Due to the lack of data, it is assumed the operations (positioning and removing) on distribution media and peel ply takes the same time. Also operations (positions and removing) on resin injection lines and vacuum lines take the same time. The time for each single step is calculated, which adds up to a total time of 6898 minutes.

Table 3.2: Manufacturing process procedures and time

| **Process** | **Process step** | **Time (minute)** |
|---|---|---|
| Mold setup | Cleaning mold | 107.2 |
| | Applying mold release to mold | 35.8 |
| | Positioning distribution media to the mold | 56.7 |
| | Positioning peel ply layer above distribution media | 56.7 |
| Hand layup | Laying up fabrics on the mold | 1248.5 |
| | Wrapping core foam beams with glass fiber fabrics | 2989.5 |
| | Applying clamping force straps and positioning beams (wrapped core foam) into mold | 403.2 |
| | Laying up fabrics over beams | 1153.5 |
| | Positioning peel ply layer | 81.5 |
| | Positioning distribution media | 81.5 |
| Machine setup & applying vacuum | Cleaning mold | 107.2 |
| | Applying mold release to mold | 35.8 |
| | Positioning distribution media to the mold | 56.7 |
| | Positioning peel ply layer above distribution media | 56.7 |
| Injection & cure | Injecting resin and monitoring the process | 181 |
| | Curing the part in mold | NA |
| | Removing the vacuum bag | 24.9 |
| Demolding | Removing injection line | 5.8 |
| | Removing vacuum lines | 5.8 |

Continued on next page

**Table 3.2 – continued from previous page**

| Process | Process step | Time (minute) |
|---|---|---|
| | Removing distribution media and peel ply | 335.1 |
| Post cure | Part post cure | NA |

Few assumptions regarding the manufacturing process should be mentioned, which include that the fiberglass fabrics (0.35 mm) and foam cores are prepared in advance, curing the part in mold and post cure require no labor time, and when the vacuum being pulled, the worker is performing other tasks.

### 3.3.4 Time cost comparison

The construction time of the basic structure of the composites hatch covers using VARTM is 6898 minutes while the construction time using hand layup in [4] is calculated to be 7424 minutes. In comparison, VARTM achieves higher structure quality and the construction time decease of about 7%.

## 3.4 Strength and stiffness comparison

Strength requirements are essential to protect the cargo beneath hatch covers. Both steel and composites hatch covers are further analyzed in term of stiffness and strength in ABAQUS. This analysis is intended to provide an insight on the method used to design the hatch cover. The homogenized properties of GFRP, steel and foam properties are provided in Table 3.3. For the steel hatch cover, 88440 C3D8R brick elements

are used. For composites hatch cover, 166400 S4R shell elements are used for composites skin. 153600 C3D8R brick elements and 437760 C3D6 wedge elements are used for the cores. Both end faces and both side edges are simply supported. The weights and maximum displacements of two hatch covers under self-weight is compared in Table 3.4. The maximum normal stresses of steel and GFRP are compared with their ultimate strength in Table 3.5.

Table 3.3: Material properties

| Material | Steel | GFRP(homogenized) | Core |
|---|---|---|---|
| Density (kg/m$^3$) | 7850 | 1800 | 32 |
| Youngs modulus (GPa) | 210 | 20 | $8.6\times10^{-3}$ |
| Poissons ratio | 0.29 | 0.28 | 0.35 |

In table 3.4, a weight saving of 38.7% is achieved by the composites hatch cover. The weight advantage will make opening and closing operation easier. The maximum deflection of composite hatch cover is 32% less compared to the steel one. For GFRP, the maximum normal stress to ultimate strength ratio is 0.005, much less than a corresponding value of 0.062 for steel. It is obvious that the composite hatch cover is stiffer. The design in [4] is not performed to optimize the composites hatch cover. Hence both the material and labor costs are expected to be reduced by optimizing the structure

Table 3.4: Deflection and weight comparison of two hatch covers

| | Steel hatch cover | Composites hatch cover |
|---|---|---|
| Weight (Kg) | 1372.78 | 841.83 |
| Max deflection (mm) | 0.19 | 0.13 |

Table 3.5: Stress comparison of steel and GFRP

| | Steel | GFRP |
|---|---|---|
| Ultimate strength (MPa) [4] | 250 | 220 |
| Maximum normal stress (MPa) | 15.39 | 1.02 |

## 3.5 Conclusion

The labor cost of manufacturing a hatch cover with VARTM is estimated using a modified cost model and framework. The construction time is then estimated using the same criteria as in [4]. The results demonstrate that less construction time cost is needed if VARTM is used for the manufacturing. Besides, comparison of strength and stiffness illustrates that better structural aspects are accomplished with composites. In conclusion, the composites hatch cover is over-designed and has the potential to be optimized, as a results of which, both weigh and cost will be further reduced. The feasibility of composite cargo ships deserves being reinvestigated carefully.

# Chapter 4

# Buckling of column on Pasternak foundation with rotational end restraints: analytical solutions and application

***Peng Yu, Sam Nakhla***

Faculty of Engineering and Applied Science

Memorial University of Newfoundland

St. John's, Newfoundland, Canada

**Keywords:** column buckling, rotational end constraints, Pasternak foundation.

***Abstract:*** *The web core sandwich structure subjected to compressive loads perpendicular to the webs has the susceptibility to buckling within a unit cell. The buck-*

*ling behavior of the unit cell under compression loading can be modeled as the elastic buckling of columns resting on the Pasternak foundation with rotational restraints at two ends. In this paper, the effects of the Pasternak foundation and rotational end restraints existing simultaneously on the critical buckling load are investigated. An analytical approximation technique, variational iteration method (VIM) is applied. Based on solving the characteristic equation, exact solutions are also presented to validate the VIM solutions. The results indicate the great significance of elastic foundations in increasing the stability. The effects of boundary conditions on critical buckling load are trivial only when stiff foundations are used. The determination of foundation parameters are provided and evaluated. The importance of web-pitch to face-sheet thickness ratio is found. Longer web-pitches are desired to increase critical loads, which also help the structure weight optimization since fewer webs are needed for a given total width. The novelties of current work include the application of variational iteration algorithm to the problem, the investigations and comparisons of combinational effects of elastic foundations and rotational restraints, the evaluations of foundation parameters based on practical materials and suggestion on the structure design.*

A version of this paper is in preparation for publication. The lead author will be Peng Yu and the co-authors will be Dr. Sam Nakhla. Mr. Yu's contribution to this paper is as follows:

- Initialized the research idea.
- Implemented the variational iteration method to solve the problem.
- Conducted numerical evaluations using MATLAB.

- Analyzed the results.
- Wrote the paper.

Dr. Nakhla provided technical guidance, suggested improvement ideas and edited the manuscript. In this chapter, the manuscript is presented with altered figure numbers, table numbers and reference formats in order to match the thesis formatting guidelines set out by Memorial University.

## 4.1 Introduction

The buckling of columns on elastic foundations is drawing wide interests from many researchers in various fields since it represents numerous practical applications [52, 53, 54, 55]. The exploration of column buckling has a long history and has been systematically explained in well-known literatures [56, 26, 57]. After the Winkler elastic foundation model first proposed [58], more sophisticated and practical foundation models were presented [59, 60, 61, 62], one of which, the Pasternak model, was demonstrated to be applicable to many problems.

Focusing on the column resting on elastic foundations, Sundararajan [63] studied the stability problem of columns on elastic foundations subjected to conservative and non-conservative forces. The Winkler's model was used and the influences of the foundation were investigated. A finite element method for the vibration of beam-column on two-parameter elastic foundation was presented by Yokoyama [64]. The finite element method was shown to be effective, and comprehensive parameter studies were then performed. Morfidis and Avramidis [65] proposed a generalized finite element for the beam-column on elastic foundations. Effects of shear deformations, semi-rigid connections, rigid offsets and axial forces could be included in the elements. A two-parameter elastic foundation model was used in their research. Post-buckling analysis of an elastic column on the Winkler foundation was performed with the employment of an approximate analytic technique [66]. The responses of perfect and geometrically imperfect columns were discussed.

For beams and plates on elastic foundations, Feng and Robert [67] suggested a finite element method to analyze beams on two-parameter foundations. Two types of

beam elements were formulated and compared. It was shown that elements based on the exact displacement function predict the results more accurately and were computationally cheaper. Levy [68] proposed a weight minimization method for beams and plates on elastic foundations for given buckling loads and optimality criteria was derived using the variational method. The buckling of simply supported laminates on Pasternak foundations subjected to uniaxial and biaxial in-plane loads was investigated by Xiang *et al* [69]. The first-order shear deformation plate theory was employed in their research. Calculus of variations was applied to minimize the total potential energy functional and the characteristic eigenvalue equation was derived based on the Navier method. Numerical results were obtained, based on which, comprehensive parameter studies were conducted. Lam *et al* [70] presented canonical exact solutions for elastic bending, buckling and vibration of isotropic plates on two-parameter foundations. Green's functions were used in the paper and the plates were limited to the Levy type. Web core sandwich panels under in-plane compression were analyzed and optimized for the minimum weight considering instability failure criteria in [71]. The web boundaries of each unit cell was assumed to be simple support to provide conservative results and the core was modeled as a one-parameter elastic foundation, which was modeled as linear elastic spring. The effects of foundations were clearly demonstrated. Similar research was carried out by Yu [72] for Levy plates on a one-parameter foundation. Exact solutions were obtained for both uniaxial and biaxial loads. Buckling of steel beam column on Pasternak foundations with simply supported - simply supported and clamped-clamped boundary conditions were investigated in [73]. The high order mode coupling was found and was symbolically determined for the former boundary condition. In terms of the determination

of foundation parameters, Sironic [74] reevaluated the foundation constants using the Airy stress function with the plane strain assumption and the principle of minimum total potential energy. Modified foundation parameters were suggested for deep and shallow elastic foundations. Recently, Briscoe [75] examined the shear buckling of isotropic plates on Pasternak foundations. A new model for the foundation parameters was proposed with the application minimum total potential energy principle.

Variational iteration method (VIM) is powerful in solving problems related to differential equations. The buckling of non-uniform column with rotational end restraints were investigated with the application of VIM [76], which was demonstrated to be an efficient tool to solve differential equation and boundary value problems [77, 78]. The same method was used in the research on the buckling of the Euler column with continuous elastic restraints [79]. The continuous elastic restraints were modeled as elastic linear springs and several combinations of boundary conditions were investigated.

It can be seen from the literature review above that combinational effects of rotational restraints and elastic foundations, which are common and realistic in engineering structures, have not been investigated. In this paper, the buckling analysis of columns on two-parameter Pasternak foundations with rotational end restraints are performed. The characteristic eigenvalue equation for the present problem is derived. The variational iteration method (VIM) is used to find the approximate solutions. The exact solutions are also provided to verify the approximate solutions. The effects of rotational spring stiffness, elastic foundation parameters and the combined effects of both are demonstrated. Parameter studies on the foundation parameters are presented. Furthermore, the methods are applied to the buckling of web core sandwich

panel subjected to compressive loads normal to webs.

## 4.2 Buckling model

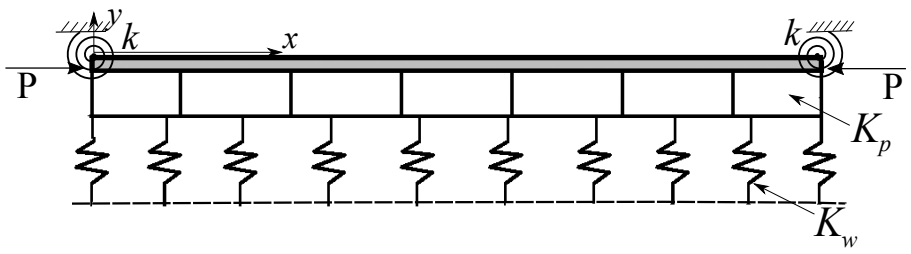


Figure 4.1: Column on the elastic foundation with rotational end restraints

Consider an Euler beam column of length $L$ and thickness $t$ resting on a two-parameter foundation with rotational springs of stiffness constants $k$, acting on two ends, Figure 4.1. The elastic modulus of the column is $E$, the second moment of area is $I$ and the flexural rigidity is $D = EI$. The two foundation parameters are $K_w$, the Winkler foundation parameter, which describes the foundations as a series of linear elastic springs normal to the beam, and $K_p$ which describes the interactions between springs. The beam column is subjected to compressive force, P. According to [73, 80], the deflection of the beam $\bar{w}(\bar{x})$ in the y direction is governed by

$$D\frac{d^4}{d\bar{x}^4}\bar{w}\left(\bar{x}\right) + P\frac{d^2}{d\bar{x}^2}\bar{w}\left(\bar{x}\right) + K_w\bar{w}\left(\bar{x}\right) - K_p\frac{d^2}{d\bar{x}^2}\bar{w}\left(\bar{x}\right) = 0 \tag{4.1}$$

For computation ease and convenience, the equation above is rewritten in the non-dimensional form as

$$\frac{d^4}{dx^4}w\left(x\right) + \pi^2\left(p - \kappa_p\right)\frac{d^2}{dx^2}w\left(x\right) + \pi^4\kappa_w w\left(x\right) = 0 \tag{4.2}$$

where $w$ is the function with respect to $x$ ($x = \bar{x}/L$). Other non-dimensional parameters shown in the equation above are

$$p = \frac{PL^2}{\pi^2 D} \qquad \kappa_p = \frac{K_p L^2}{\pi^2 D} \qquad \kappa_w = \frac{K_w L^4}{\pi^4 D} \tag{4.3}$$

For the non-dimensional differential equation, the boundary conditions at $x = 0$ are

$$\frac{d^2}{dx^2} w\,(0) = \kappa \frac{d}{dx} w\,(0)\,, \qquad w(0) = 0 \tag{4.4}$$

and the boundary conditions at $x = 1$ are

$$\frac{d^2}{dx^2} w\,(1) = -\kappa \frac{d}{dx} w\,(1)\,, \qquad w(1) = 0 \tag{4.5}$$

The non-dimensional parameter $\kappa$ in Equation 4.4 and 4.5 is

$$\kappa = \frac{kL}{D} \tag{4.6}$$

According to [57], the general solution to equation 4.2 is

$$w\,(x) = C_1 \cos\,(\beta_1 x) + C_2 \sin\,(\beta_1 x) + C_3 \cos\,(\beta_2 x) + C_4 \sin\,(\beta_2 x) \tag{4.7}$$

where

$$\beta_1 = \sqrt{\frac{\alpha}{2} - \sqrt{\frac{\alpha^2}{4} - \xi}} \qquad \beta_2 = \sqrt{\frac{\alpha}{2} + \sqrt{\frac{\alpha^2}{4} - \xi}} \tag{4.8}$$

$$\alpha = \pi^2 (p - \kappa_p) \qquad \xi = \pi^4 \kappa_w \tag{4.9}$$

and $C_1$, $C_2$, $C_3$ and $C_4$ can be determined according to boundary conditions. Equation 4.8 holds when $\frac{\alpha^2}{4} - \xi \geqslant 0$, which gives $p \geqslant \kappa_p + 2\sqrt{\kappa_w}$. Substituting the $w(x)$

in Equation 4.4 and 4.5 with the $w(x)$ form Equation 4.7 leads to the characteristic equation for this problem.

## 4.3 Variational iteration method

VIM is an analytical approximation technique. It is widely used in solving nonlinear differential equations with the advantages of effectiveness, accuracy and converging to exact solutions rapidly [78]. Considering a homogeneous nonlinear differential system as follows:

$$L[w(t)] + N[w(t)] = 0 \tag{4.10}$$

where $L$ is a linear operator and $N$ is a nonlinear operator.

To solve the nonlinear differential equation above using VIM, a correction function should be constructed. According to He *et al* [78], three iteration formulas are commonly used, including

$$w_{n+1}(x) = w_n(x) + \int_0^x \lambda(\zeta)(L[w_n(\zeta)] + N[\tilde{w}_n(\zeta)])d\zeta \tag{4.11}$$

$$w_{n+1}(x) = w_0(x) + \int_0^x \lambda(\zeta)N[w_n(\zeta)]d\zeta \tag{4.12}$$

$$w_{n+2}(x) = w_{n+1}(x) + \int_0^x \lambda(\zeta)(N[w_{n+1}(\zeta)] - N[w_n(\zeta)])d\zeta \tag{4.13}$$

where $\lambda$ is a general Lagrange multiplier that can be identified optimally via variational theory, $w_0$ is the initial guess and $w_n$ is the n-th approximate solution and $\tilde{w}_n$ denotes a restricted variation [77, 78]. Equation 4.11, 4.12 and 4.13 are variational iteration algorithm I, II and III, respectively. The initial guess $w_0$ in algorithm II

is required to satisfy the boundary conditions, which is complicated in the present problem due to the existence of the restraints at the ends. Thus, the simpler algorithm I is chosen. For a four order differential equation, a simple Lagrange multiplier is suggested in [76] as

$$\lambda(\zeta) = \frac{(\zeta - x)^3}{6} \tag{4.14}$$

With the Lagrange multiplier, the correction function for the present problem is represented as

$$w_{n+1}(x) = w_n(x) + \int_0^x \frac{(\zeta - x)^3}{6} \left(\frac{d^4}{d\zeta^4} w_n(\zeta) + \pi^2 (p - \kappa_p) \frac{d^2}{d\zeta^2} w_n(\zeta) + \pi^4 \kappa_w w_n(\zeta)\right) d\zeta \tag{4.15}$$

The initial solution $w_0$ of the deflection function of the beam can be freely selected and unknown parameters can be contained in it. The initial solution is chosen to be a polynomial, which is

$$w_0(x) = Ax^3 + Bx^2 + Cx + D \tag{4.16}$$

With the initial solution and the correction function, iterations can be conducted. MATLAB is used to facilitate computations. After the nth iterations, an approximate solution is obtained, which will be substituted into the boundary conditions, Equation 4.4 and 4.5. Correspondingly, four homogeneous equations are obtained from the four boundary conditions and the characteristic equation is derived by making the determinant of coefficient matrix of the four homogeneous equations zero. The accuracy of VIM is related to iteration times.

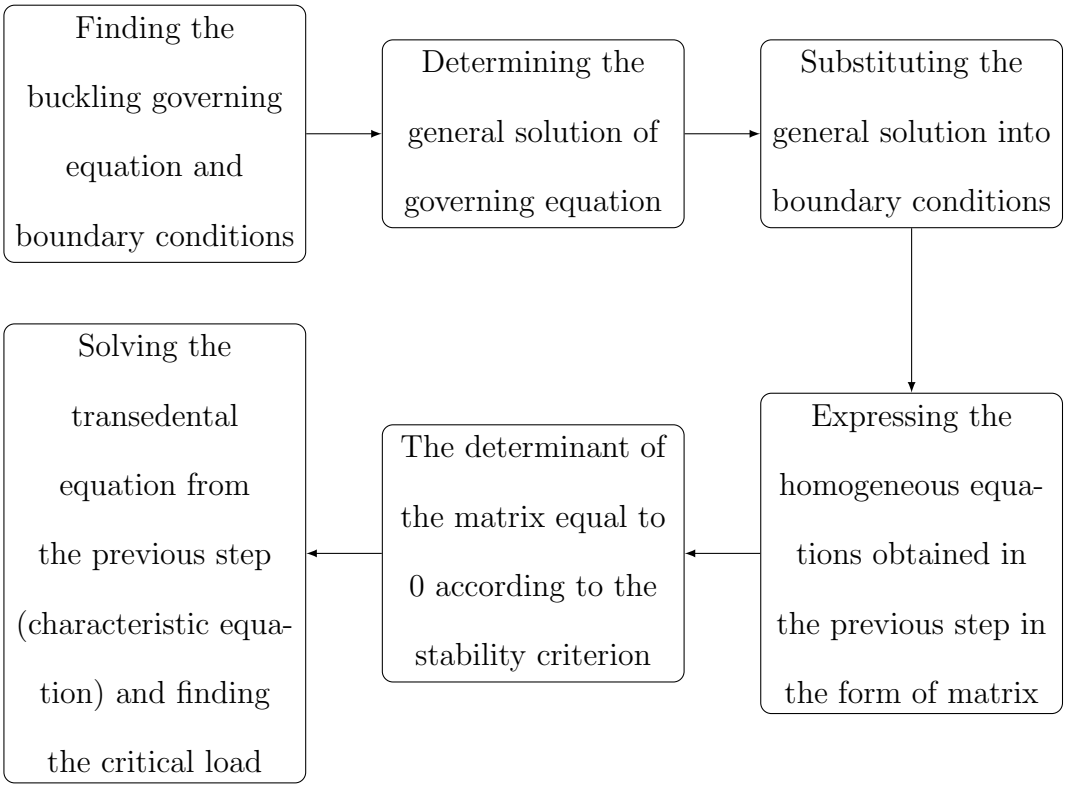


Figure 4.2: Flow chart of finding exact solutions

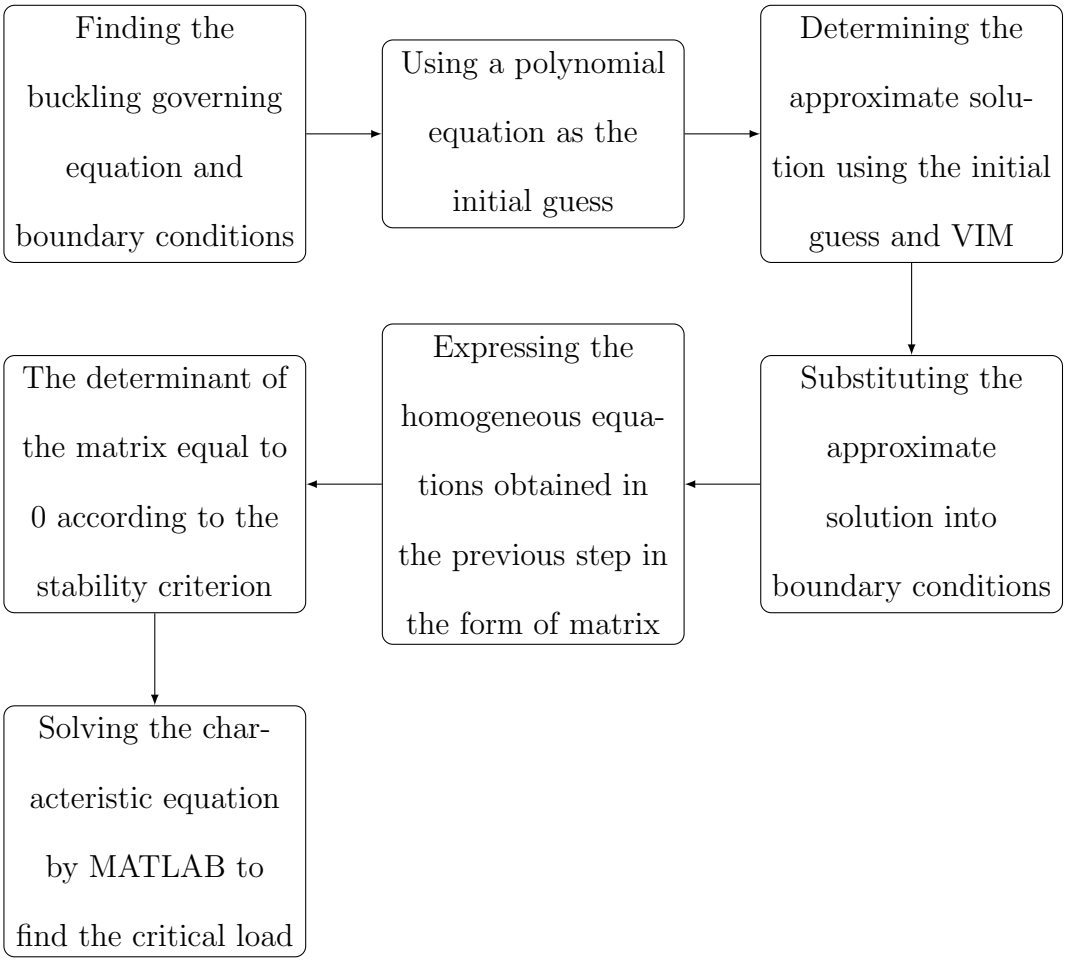


Figure 4.3: Flow chart of finding VIM solutions

## 4.4 Numerical evaluations and discussion

Numerical evaluations of the characteristic equation from Section 4.2 and the characteristic equation of the approximate solution from VIM are performed. The flow charts for finding exact and VIM solutions are illustrated in 4.2 and 4.3, respectively. The procedures in Figure 4.3 are implemented in MATLAB and the critical load is easily found by MATLAB. As mentioned above, no literatures have been published regarding this problem. A special case, i.e. column with rotational end restraints without elastic foundation is evaluated and compared with the results in the literature. The numerical evaluation of the case is achieved by setting the foundation parameters to zero. In this paper, the rotational restraints at two ends are made equal, which is practical for most web core sandwich structures. Obviously, non-equal restraints situations can also be calculated using the two method presented in this paper.

It can be seen from Table 4.1 that the approximate analytical solutions after 10 iterations using VIM are close to the exact solutions with high degree of accuracy. Then, approximate and exact buckling solutions of column on Winkler's and Pasternak's foundations are computed and the results are shown in Table 4.2 and 4.3. The range of normalized stiffness constants of rotational restraints is from 0.1 to infinity ($10^9$). Different ratios of two foundation parameters are chosen in Table 4.3. The computation of 25 iterations is conducted in the VIM. The approximate solutions are extremely close or identical to the exact solutions. The feasibility and accuracy of VIM are further illustrated. The solutions provided in the two tables can be used as benchmarks for other numerical methods for this problem.

Table 4.1: Comparison of present exact and VIM solutions with those in literatures

| $\kappa$ | VIM(n=10) | Wang[57]$^{\dagger}$ |
|---|---|---|
| 0 | 1 | 1 |
| 0.5 | 1.1927 | 1.1928 |
| 1 | 1.3671 | 1.3670 |
| 2 | 1.6681 | 1.6681 |
| 4 | 2.1234 | 2.1234 |
| 10 | 2.8540 | 2.8540 |
| $\infty$ | 3.9999 | 4 |

$^{\dagger}$ Due to different method of normalization, the values in the table are obtained by dividing the results in [57] by $\pi^2$

### 4.4.1 Effects of rotational end restraints and elastic foundation on buckling load

A parameter study on the normalized rotational spring constant $\kappa$ is presented first. For the sack of brevity, the elastic foundation is absent and the normalized critical load is found for different normalized rotational spring constants, as illustrated in Figure 4.4. To show the results explicitly, the $lg(\kappa)$ scale is generated for the $x$ axis. Apparently, the normalized critical load increases slowly when $\kappa$ exceeds 100 ($lg(\kappa) = 2$). When the normalized rotational spring constant is 10000, the normalized critical load is almost 4 (3.9986 form the exact solution and 4.006 from VIM), which is the

Table 4.2: Exact and approximate solutions (Winkler foundations)

| | | $\kappa_w$=1, $\kappa_p$=0 | $\kappa_w$=10, $\kappa_p$=0 | $\kappa_w$=100, $\kappa_p$=0 | $\kappa_w$=150, $\kappa_p$=0 | $\kappa_w$=300, $\kappa_p$=0 |
|---|---|---|---|---|---|---|
| $\kappa = 0.1$ | Exact | 2.0401 | 6.5402 | 20.1513 | 25.4152 | 34.7902 |
| | VIM | 2.0401 | 6.5402 | 20.1513 | 25.4152 | 34.7956 |
| $\kappa = 1$ | Exact | 2.3644 | 6.8734 | 20.4815 | 25.7472 | 35.1213 |
| | VIM | 2.3644 | 6.8734 | 20.4815 | 25.7472 | 35.1231 |
| $\kappa = 10$ | Exact | 3.7658 | 8.5731 | 22.0763 | 27.2434 | 36.7527 |
| | VIM | 3.7658 | 8.5731 | 22.0763 | 27.2434 | 36.7130 |
| $\kappa = 10^2$ | Exact | 4.6157 | 9.9614 | 23.2506 | 27.8283 | 38.0160 |
| | VIM | 4.6157 | 9.9614 | 23.2506 | 27.8283 | 37.9560 |
| $\kappa = 10^4$ | Exact | 4.7419 | 10.1973 | 23.4401 | 27.9069 | 38.2264 |
| | VIM | 4.7419 | 10.1973 | 23.4401 | 27.9069 | 38.1754 |
| $\kappa = \infty$ | Exact | 4.7432 | 10.1998 | 23.4420 | 27.9077 | 38.2286 |
| | VIM | 4.7432 | 10.1998 | 23.4420 | 27.9078 | 38.1778 |

Table 4.3: Exact and approximate solutions (Pasternak foundations)

| | | $\kappa_w$=1, $\kappa_p$=0.01 | $\kappa_w$=10, $\kappa_p$=2 | $\kappa_w$=100, $\kappa_p$=10 | $\kappa_w$=150, $\kappa_p$=50 | $\kappa_w$=300, $\kappa_p$=50 |
|---|---|---|---|---|---|---|
| $\kappa = 0.1$ | Exact | 2.0501 | 8.5402 | 30.1513 | 75.4152 | 84.7902 |
| | VIM | 2.0501 | 8.5402 | 30.1513 | 75.4152 | 84.7956 |
| $\kappa = 1$ | Exact | 2.3744 | 8.8734 | 30.4815 | 75.7472 | 85.1213 |
| | VIM | 2.3744 | 8.8734 | 30.4815 | 75.7472 | 85.1231 |
| $\kappa = 10$ | Exact | 3.7758 | 10.5731 | 32.0763 | 77.2434 | 86.7529 |
| | VIM | 3.7758 | 10.5731 | 32.0763 | 77.2434 | 86.7130 |
| $\kappa = 10^2$ | Exact | 4.6257 | 11.9614 | 33.2506 | 77.8283 | 88.0160 |
| | VIM | 4.6257 | 11.9614 | 33.2506 | 77.8283 | 87.9560 |
| $\kappa = 10^4$ | Exact | 4.7519 | 12.1973 | 33.4401 | 77.9069 | 88.2264 |
| | VIM | 4.7519 | 12.1973 | 33.4401 | 77.9069 | 88.1754 |
| $\kappa = \infty$ | Exact | 4.7532 | 12.1998 | 33.4420 | 77.9077 | 88.2286 |
| | VIM | 4.7532 | 12.1998 | 33.4420 | 77.9078 | 88.1777 |

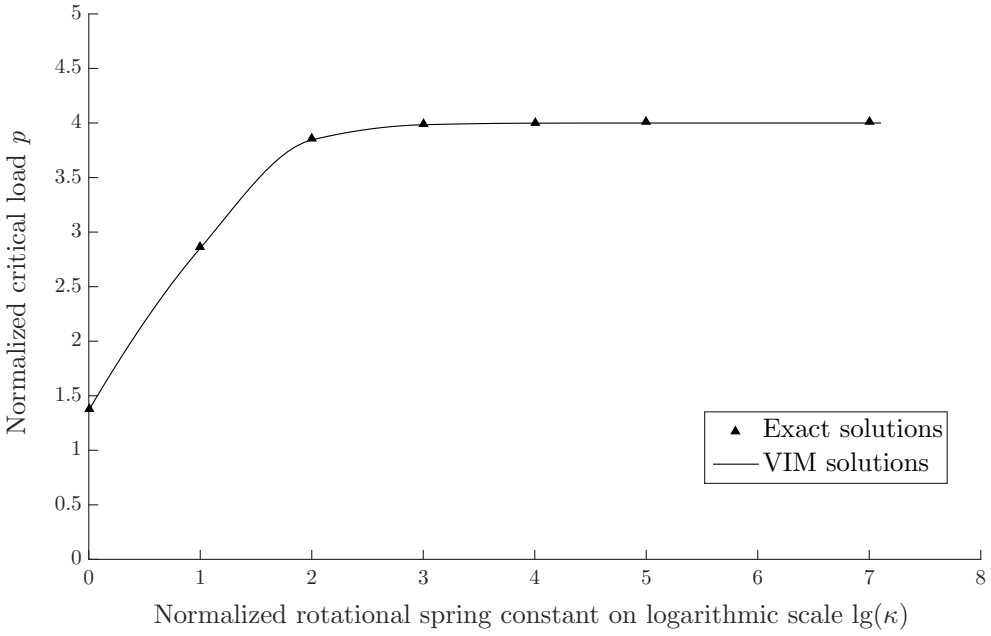


Figure 4.4: Column without elastic foundations

normalized critical load for the clamped-clamped boundary condition. The critical load merely increases when $k$ exceeds 10000. In the later part of this paper, $\kappa = 10^4$ is regarded as the clamped-clamped boundary condition to facilitate computations and explanations. This will hold for both the columns with or without elastic foundations with the assumption that the rigidity of rotational springs is not influenced by the existence of core.

The combinational effects of rotational end restraints and foundation parameters are demonstrated then. Normalized rotational spring constants from 1 to 10000 and various foundation parameter ratios, i.e. $\kappa_w/\kappa_p = 5$, 15 and 25 with the range 0 to 300 of $\kappa_w$, are covered to achieve generalities. The numerical results are shown in Figure 4.5, 4.6 and 4.6. Obviously, The incorporation of foundations increases the critical buckling loads dramatically. The four lines representing different normalized

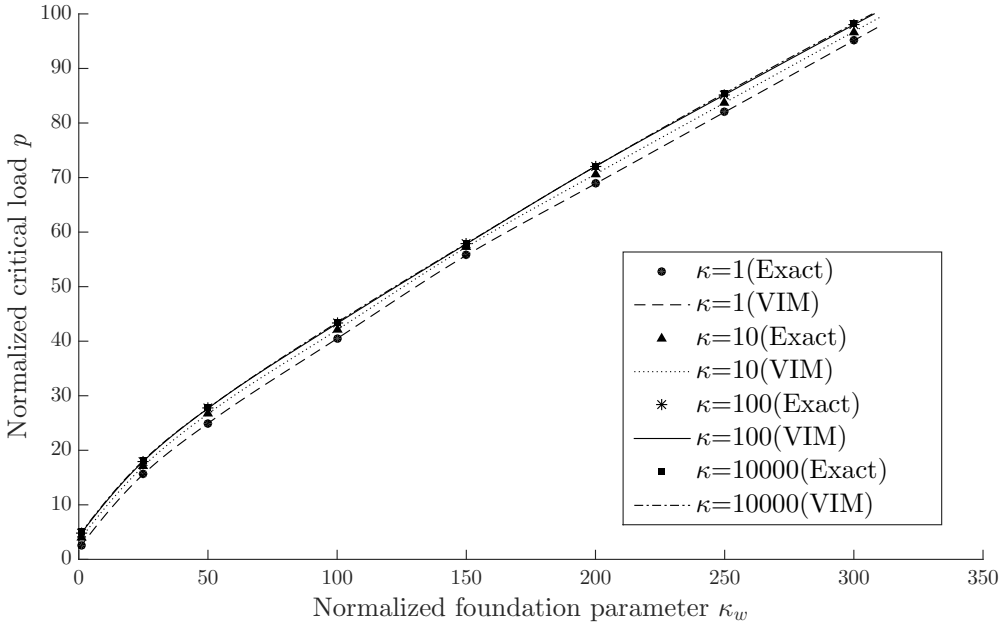


Figure 4.5: Buckling of column on elastic foundations ($\kappa_w/\kappa_p = 5$)

rotational spring constants are close to each other, which is true for all the three different foundation parameter ratios. The lines are approaching linear and parallel to each other with the increase of foundations parameters. It implies that the effects of foundation parameters are dominant when the foundations are strong, while rotational restraints have more significant effects when the foundations are weaker. To further demonstrate the effect of rotational springs for various foundation parameters, the increasing percentage of critical load compared with column on elastic foundation with pin-pin boundary conditions are shown in Figure 4.8. The increase of critical load is significant, over 70%, for small foundation parameters (weak foundation) while that for large foundation parameters (strong foundation) is neglectable since the maximum increase is around 5%.

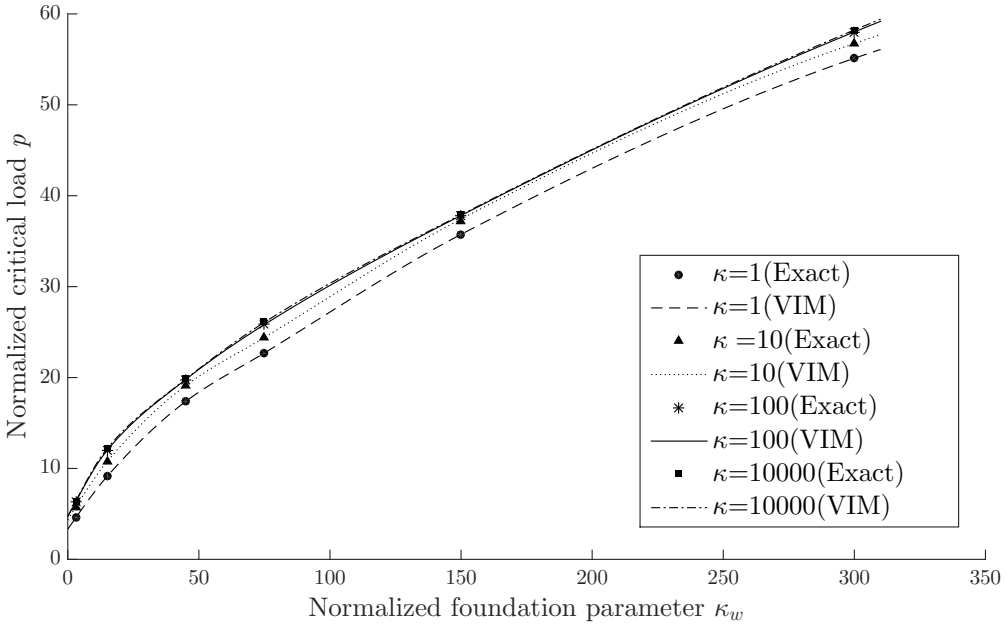


Figure 4.6: Buckling of column on elastic foundations ($\kappa_w/\kappa_p = 15$)

## 4.5 Application to web core sandwich structure

The sandwich structure is extensively used in many engineering industries, such as aerospace, ocean and building industry, due to the advantageous properties of high stiffness, light weight and design effectiveness [81]. Web core sandwich structures consist of two face-sheets connected and supported by interior webs, and core bonded to the face-sheets and webs. Web core sandwich panel have been applied to large ship structures and residential building roof to satisfy special requirements [53, 75, 82]. The improvement of shear property and fatigue life of web core sandwich structures can be achieved with the use of core materials [83, 84].

From the analysis above, it can be seen that modeling the webs as simply-supported or clamped boundary conditions can be simplistic and introduces sig-

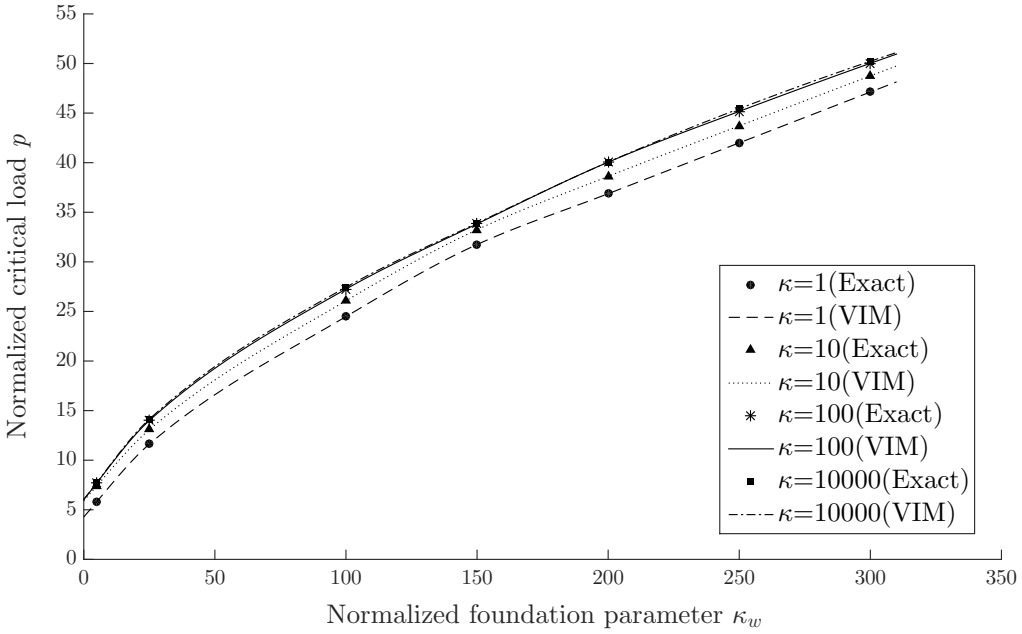


Figure 4.7: Buckling of column on elastic foundations ($\kappa_w/\kappa_p = 25$)

nificant errors. A practical method is to discrete webs and face-sheets and model webs as rotational restraints. The effect of rotational restraints on the buckling behavior of plate and beam has drawn the attention of many researchers. Lundquist and Stowell [85] obtained the exact and approximate solutions for the buckling of isotropic plates subjected to uniaxial compression and rotationally constrained along unloaded edges. Valuable data on critical buckling stresses are provided. Bleich [86] investigated the buckling of box shape under compression. The formulas of rotational constraint stiffness from the two sides of the box shape are presented. Explicit solutions for the buckling of orthotropic plate with rotational restraints using Ritz method are presented in [87, 88, 89]. The solution is applied to I section, C section, and box section *etc*. The formula to determine constraint stiffness constant in [86] is extended to orthotropic plates in their work. Significant effects of the rotational

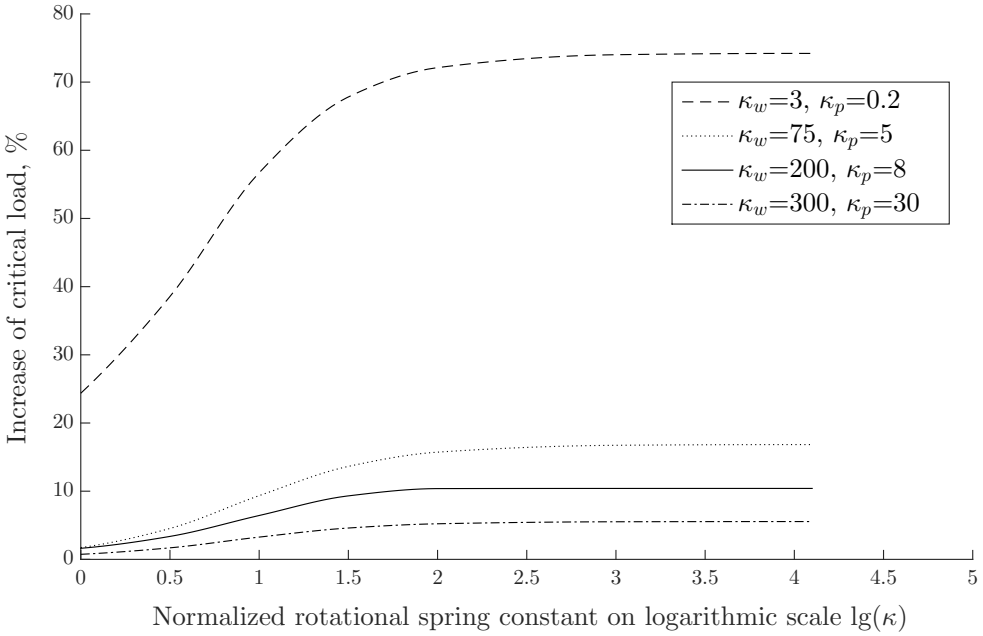


Figure 4.8: Illustration of the effect of rotational spring constants

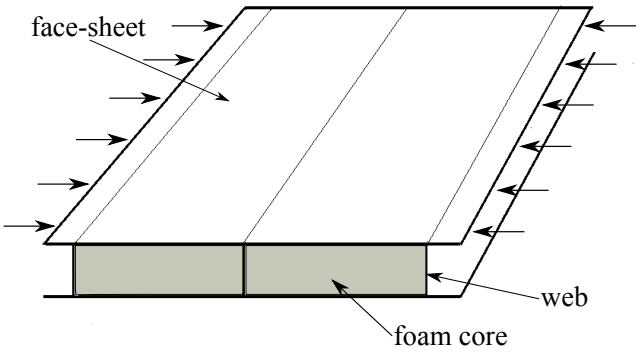


Figure 4.9: Illustrate of web core panel

restraints on local bucking are found. Similar work on the buckling of rotational restrained fiber reinforced plastic composite plates are conducted by Kollar [90, 91]. More details concerning local buckling with rotational constraints can also be found

in [92]. Furthermore, the rotational constraints are considered for the laser-welded web core sandwich plate [93]. The method to determine the rotational spring stiffness is proposed for laser welding. Linear spring and rotational spring are combined to model the general boundary conditions in [94]. Euler beam buckling with general boundary conditions are examined using Galerkin method.

The web core panel subjected to compression and bending loads is susceptible to local buckling [53], Figure 4.9. When a panel is subjected to uniformly distributed compressive loads perpendicular to webs with unloaded edges free, the constrained buckling of face-sheet, which is referred to as the buckling of face-sheets between webs, may occur [53]. Due to the periodicity, the whole panel is represented by a unit cell, Figure 4.10. The webs in the unit cell provide rotational restraints to the face-sheet and the core acts as the elastic foundation. Hence, the constrained buckling of web core sandwich panel resembles the buckling of column on elastic foundations with rotational ends restraints. The column is of unit width and accounts for Poisson's ratio effects [95], which means the flexural rigidity should be modified as $D_p = EI/(1-\nu^2)$.

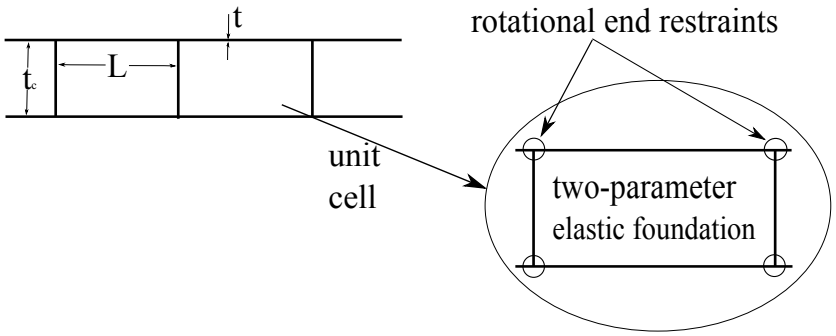


Figure 4.10: Cross section of web core sandwich panel and unit cell

### 4.5.1 Evaluation of foundation parameters of typical core material

The foundation parameters have significant effects on the critical buckling load. Therefore, the foundation parameters are further evaluated to give a insight of them and the evaluations are based on practical web core sandwich geometries. Research on the determination of the two foundation parameters are available in [74, 96]. In many web core sandwich panels, the thickness of core is relatively small compared to the web-pitch, which means the core is shallow. For shallow foundations, the determination of parameters are provided in [97] and different equations are proposed in [53]. The latter, as Equation 4.17, is used here because they have been validated by finite element analysis. Normalized foundation parameters are expanded and expressions with respect to the structure geometries and material properties are obtained, Equation 4.18,

$$k_w = \frac{E_c}{6t_c} \qquad k_p = \frac{G_c t_c}{3} \tag{4.17}$$

$$\kappa_w = \frac{2}{\pi^4}\gamma\chi^3\eta_E \qquad \kappa_p = \frac{4}{\pi^2}\tau\chi^2\eta_G \tag{4.18}$$

where $\eta_E$ is the ratio of core elastic modulus to column elastic modulus $E_c/E$, $\eta_G$ is the ratio of core shear modulus to column elastic modulus $G_c/E$, $\gamma$ is the ratio of column length to core thickness $L/t_c$, $\tau$ is the ratio of core thickness to column thickness and $t_c/t$ and $\chi$ is the ratio of column length to thickness $L/t$. The equation shows the use of core material with higher elastic and shear modulus is advantageous. However, stiffer material is usually denser, which will increase the structure weight. $\kappa_w$ and $\kappa_p$ are proportional to the cubic and square of length to thickness ratio, respectively, so

for a constant column thickness, increasing the column length (web-pitch) leads to higher buckling loads.

The typical web-pitch length used in marine industries is 120 mm and the core thickness is 40 mm. To explicitly demonstrate the effect of geometric parameters, different pitch lengths and core thicknesses are evaluated. The pitch lengths include 120 mm, 160 mm and 200 mm and the core thickness include 30 mm, 40 mm and 50 mm. The thickness of the column remains 2 mm. In practice, the filling foam material can be soft and light or rigid and dense. Various foams can be chosen according to the requirements of different applications. Four foams with different densities and mechanical properties are selected, which include rigid Polyurethane foam and Divinycell H-grade foam H45, H100 and H250. The property parameters of the foams are listed in Table 4.4. The normalized foundation parameters corresponding to different foam and geometry combinations are obtained, Table 4.5.

Table 4.4: Foam core properties

| property | PU [75] | H45 [83] | H100 [83] | H250 [83] |
|---|---|---|---|---|
| density [kg/m$^3$] | 32 | 45 | 100 | 250 |
| elastic modulus [MPa] | 5.17 | 45 | 115 | 240 |
| shear modulus [MPa] | 1.58 | 12 | 28 | 88 |

In Table 4.5, it can be seen that for the same pitch length, $\kappa_w$ decreases with the increase of core thickness while $\kappa_p$ increase with the increase of core thickness for all the foams. For the same core thickness, $\kappa_w$ becomes dramatically large for long pitch and $\kappa_p$ also increase apparently. The results are identical with the predictions

Table 4.5: Normalized foundation parameters for different foams and geometries

| $t_c$ [mm] | | 30 | | | 40 | | | 50 | | |
|---|---|---|---|---|---|---|---|---|---|---|
| L [mm] | | 120 | 160 | 200 | 120 | 160 | 200 | 120 | 160 | 200 |
| Rigid PU | $\kappa_w$ | 0.4474 | 1.4140 | 3.4520 | 0.3355 | 1.0605 | 2.5890 | 0.2684 | 0.8484 | 2.0712 |
| | $\kappa_p$ | 0.1687 | 0.2999 | 0.4685 | 0.2249 | 0.3998 | 0.6247 | 0.2811 | 0.4998 | 0.7809 |
| H45 | $\kappa_w$ | 3.8941 | 12.3072 | 30.0468 | 2.9205 | 9.2304 | 22.5351 | 2.3364 | 7.3843 | 18.0281 |
| | $\kappa_p$ | 1.2811 | 2.2775 | 3.5586 | 1.7081 | 3.0367 | 4.7448 | 2.1352 | 3.7958 | 5.9310 |
| H100 | $\kappa_w$ | 9.9515 | 31.4516 | 76.7862 | 7.4636 | 23.5887 | 57.5897 | 5.9709 | 18.8710 | 46.0717 |
| | $\kappa_p$ | 2.9892 | 5.3142 | 8.3034 | 3.9856 | 7.0856 | 11.0712 | 4.9820 | 8.8570 | 13.8390 |
| H250 | $\kappa_w$ | 20.7683 | 65.6382 | 160.2495 | 15.5762 | 49.2286 | 120.1871 | 12.4610 | 39.3829 | 96.1497 |
| | $\kappa_p$ | 9.3947 | 16.7017 | 26.0964 | 12.5263 | 22.2689 | 34.7952 | 15.6578 | 27.8361 | 43.4940 |

by Equation 4.18.

Based on the normalized foundation parameters, the critical buckling load of column with clamped-clamped boundary conditions ($\kappa = 10^4$) is evaluated, Table 4.6. For the same pitch length, the critical loads are close for Rigid PU, H45 and H100 although the thickness are different, which means the effect of panel thickness is insignificant in this range. The thickness has larger influences with the application of the H250. This finding is desired for engineering design when the soft core is used because the smaller thickness can be used to reduce the structural weight. It is also found that for the same core thickness, the pitch length has significant effect. The effect of foams properties are also evident. Some values concerning beam buckling on soft and stiff core with SS and CC boundary conditions are listed in Table 4.7. For some conditions such as long pitch and stiffer core, the effect of boundary conditions can be ignored due to their trivial influence. For example, when the web-pitch of 200 mm and the core thickness of 30 mm and H250 are used as core material, the critical load with pin-pin boundary conditions is 52.1120 while that of clamped-clamped boundary conditions is 54.8823. The difference is less than 5%. The rotational restraints can be treated as simply supported and the results will not be too conservative. However, when short pitch and soft core is used, the rotational boundary condition should be considered. The stiffness the webs provided should be evaluated for the latter case. Within the restrictions of other design criteria, longer pitch should be used to reduce the number of web used for a given total width of panel to reduce the structure weight.

Table 4.6: Normalized critical loads for different foams and geometries

| $t_c$ [mm] | | 30 | | | 40 | | | 50 | | |
|---|---|---|---|---|---|---|---|---|---|---|
| L [mm] | | 120 | 160 | 200 | 120 | 160 | 200 | 120 | 160 | 200 |
| Rigid PU | $p$(VIM) | 4.5029 | 5.3466 | 6.9685 | 4.4758 | 5.1875 | 6.5180 | 4.4819 | 5.1312 | 6.3039 |
| | $p$(Exact) | 4.5029 | 5.3466 | 6.9685 | 4.4758 | 5.1875 | 6.5180 | 4.4819 | 5.1312 | 6.3039 |
| H45 | $p$(VIM) | 8.0864 | 12.9365 | 17.6543 | 7.8360 | 13.0828 | 17.4072 | 7.8484 | 12.8592 | 17.7174 |
| | $p$(Exact) | 8.0864 | 12.9365 | 17.6543 | 7.8360 | 13.0828 | 17.4072 | 7.8484 | 12.8592 | 17.7174 |
| H100 | $p$(VIM) | 13.1793 | 19.6739 | 29.5572 | 13.0967 | 19.9512 | 30.0451 | 13.1663 | 20.8081 | 30.8564 |
| | $p$(Exact) | 13.1793 | 19.6739 | 29.5572 | 130967 | 19.9512 | 30.0451 | 13.1663 | 20.8081 | 30.8564 |
| H250 | $p$(VIM) | 21.7151 | 36.8650 | 54.8823 | 23.8315 | 39.8359 | 60.0767 | 26.3473 | 43.6591 | 66.5791 |
| | $p$(Exact) | 21.7151 | 36.8650 | 54.8823 | 23.8315 | 39.8359 | 60.0767 | 26.3473 | 43.6591 | 66.5791 |

Table 4.7: Example of buckling load with CC and SS boundary conditions

| | | $t_c$ = 30, L=200 | $t_c$ = 40, L=160 | $t_c$ = 50, L=120 |
|---|---|---|---|---|
| Rigid PU(5.17,1.58) | CC | 6.9685 | 5.1875 | 4.4819 |
| | SS | 4.9205 | 2.4603 | 1.5495 |
| H250 | CC | 54.8823 | 39.8359 | 26.3473 |
| | SS | 52.1120 | 36.7387 | 22.7730 |

## 4.6 Conclusion

Approximate and exact solutions are presented in the paper to obtain the buckling solutions of columns resting on Pasternak foundations with rotational end restraints. The variational iteration method is used for this problem to find the approximate solution and is found convenient, efficient and accurate. The effects of rotational end restraints and Pasternak foundation parameters are investigated simultaneously. Rotational end restraints significantly increase critical buckling loads when weak foundations (foams) are used and the effects are weakened when denser and stronger foundations (foams) exists. Geometric and material properties are incorporated in the normalized foundation parameters. Practical structural geometries and foam materials are used to further evaluate foundation parameters. For some cases where long web-pitch and stiffer foams are used, the rotationally constrained boundary conditions can be simplified as simply supported without introducing large errors.

# Chapter 5

# Finite element analysis of sandwich panel face-sheet wrinkling

***Peng Yu, Sam Nakhla***

Faculty of Engineering and Applied Science

Memorial University of Newfoundland

St. John's, Newfoundland, Canada

**Keywords:** sandwich structure, wrinkling, composites, finite element analysis.

***Abstract:*** *The wrinkling of sandwich structure is a significant failure mode and should be considered in the design stage. The neglect of wrinkling may cause catastrophic failure because wrinkling can initiate other failures such as core failure and the debonding of face-sheets and core. The analytical solution of face-sheet wrinkling is proposed in the paper. The finite element analysis is employed using ABAQUS to investigate the wrinkling phenomenon. The finite element models are constructed based*

*on the geometries and materials of the testing specimens in the literature. The effect of boundary conditions on the wrinkling is revealed. The different types of elements to represent the face-sheets are attempted, and the advantages and disadvantages of different elements are discussed. It is concluded that the analytical solution presented in the paper can only predict the critical wrinkling loads accurately for the sandwich panel of specific face-sheet to core ratios. The finite element analysis is a reliable and effective tool for the prediction of critical wrinkling loads.*

A version of this paper is in preparation for publication. The lead author will be Peng Yu and the co-authors will be Dr. Sam Nakhla. Mr. Yu's contribution to this paper is as follows:

- Conducted finite element analysis using ABAQUS.
- Analyzed the results.
- Wrote the paper.

Dr. Nakhla initialized the research idea, suggested the analytical solution, provided technical guidance, and is editing of the manuscript. In this chapter, the manuscript is presented with altered figure numbers, table numbers and reference formats in order to match the thesis formatting guidelines set out by Memorial University.

## 5.1 Introduction

Sandwich structures are of great significance in engineering due to the high stiffness to weight ratio, excellent corrosion resistance and tailorable mechanical properties [81]. Typical sandwich structures comprise two face-sheets at sides and one core in the middle. The face-sheets are bonded to the core, which plays the role of providing support and stability to the face-sheets.

The sandwich failure is of interest to many researchers and engineer. The failure modes of sandwich structures include the failure of face-sheets under compressive and extensional loads,the face-sheet indentation failure under concentrated loads, core failure, the debonding of face-sheets and core, global buckling and wrinkling. Wrinkling is referred to as a face-sheet instability failure phenomenon where the wavelength of the buckled form is short and is of the same order as the core thickness [36]. It is commonly observed when compression loads are applied to the sandwich structure. Wrinkling is essential because the wrinkled face-sheets may initiate many other failure modes, such as the debonding of face-sheets and core, core failure and face-sheet failure.

Single-sided wrinkling, symmetric wrinkling and anti-symmetric wrinkling, Figure 5.1, shows the three common wrinkling modes. The first mode usually happens to sandwich structures subjected to bending loads or one face-sheet is much stiffer than the other one, while symmetric and anti-symmetric wrinkling happen to in-plane compression loading conditions. The occurrence of symmetric or antisymmetric wrinkling mode is related to the material properties and geometries of the sandwich structures.

(a) Single-sided wrinkling

(b) Symmetric wrinkling

(c) Anti-symmetric wrinkling

Figure 5.1: Three different wrinkling modes

The wrinkling failure has been investigated since the 1940s analytically, experimentally and numerically. Several famous wrinkling formulas based on different methods and assumptions have been proposed. The analytical models need to be validated by testings. However, it is not easy to conduct testing ideally due to the constraints of geometric imperfections caused by the specimen manufacturing process and the limitations from apparatus. Besides, complex failure modes and their interactions make it difficult to find the critical wrinkling load. Hence, the finite element analysis (FEA), as a simulation to the testings, provides a better solution to this problem. In this paper, both analytical method and finite element analysis are applied to investigate the wrinkling failure. The analytical solutions and FEA results are compared with that of the classic wrinkling models and testing results in

literature. The effects of boundary conditions and face-sheet element types are also examined.

## 5.2 Literature review on wrinkling research

The wrinkling of sandwich structure was investigated in [24]. In the paper, eight different combinations of face-sheets and supporting medium were studies analytically. Hoff and Mautner [25] presented buckling formulas for both symmetric and anti-symmetric modes based on the principle of minimum total potential energy. The symmetric wrinkling mode was also solved using the elasticity theory in their paper. Nardo [27] derived the exact solutions for the buckling of sandwich panel with loaded edges clamped and unloaded edges simply supported. The report [28] summarized the previous research before 1961 and reaffirmed the results with experiments. A paper based on [28] was published in [1]. In Plantema's model [29], an exponential decay of the core displacements in the transverse direction was assumed. The principle of minimum total potential energy was also applied in his model. Allen's model [31] had the same geometric assumptions as that of Plantema. The critical stress was derived by solving the governing equation with the assumption that the core stress field satisfied the Airys stress functions. Analytical, numerical and experimental investigations of face-sheet wrinkling subjected to uniaxial and biaxial compression in sandwich shell was conducted by Stiftinger and Rammerstorfer [32]. The effect of the orthotropy of face-sheet and core were investigated and it was found that anti-symmetric wrinkling was critical for face-sheets with isotropic core, and symmetric wrinkling was possible for face-sheets with the orthotropic core. Niu and Talreja [33]

presented a unified model to incorporate symmetric wrinkling and anti-symmetric wrinkling. The Winklers model was modified according to their model and the two parameter model was evaluated in their paper. The Winkler's elastic foundation approach can also be used in predicting the symmetric wrinkling load of sandwich structure, as explained in [36]. The core was modeled as elastic spring and the critical stress was derived by solving the differential governing equation. The interaction between the elastic springs, i.e. the effect of shear stress, was ignored in the approach.

Vonach and Rammerstorfer [41] presented an analytical model for the wrinkling of thick orthotropic sandwich plates boned to a transversely isotropic thick core. A 3D finite element analysis simulation using ABAQUS was used to validate the analytical model. Hadi [42] used finite element analysis to study sandwich column wrinkling and compared FEA results with the existing analytical and experimental results in [34], [37] and [38]. In the FE model, the face-sheet was modeled by 4 nodes quadrilateral elements based on the Mindlin-Reisser shell formulation. Fagerberg and Zenkert [43] investigated the reason of discrepancies between experimental and analytical results. They presented an imperfection induced wrinkling model, which includes geometric imperfections of the sinusoidal shape. The accuracy of the analytical model was also validated by finite element analysis simulation. The plane stress 2D finite element analysis simulation was conducted in ABAQUS. Periodic boundary conditions were implemented as [41]. Ji and Waas [35] investigated the global and local buckling of a sandwich beam using classical elasticity. Finite element analysis using Abaqus was applied to validate the accuracy of their model. Fleck and Sridhar [39] conducted experiments to investigate the failure mode of sandwich columns comprising of GFRP face-sheet and PVC foam core under the end compression. For the face-sheet wrin-

kling, modified Hoff's model (the coefficient was reduced to 0.5) was used as analytical solutions.

## 5.3 Analytical solutions

In the present paper, the wrinkling of the face-sheets is considered to resemble a beam resting on Winkler elastic foundation with clamped-clamped boundary conditions. A new face-sheet deformation function is presented, Equation 5.1, which satisfies the boundary conditions at the two ends of the wrinkled part. In the equation, $w_f$ represents the deformation in the transverse direction, $A$ is a constant representing the amplitude of wrinkling half-waves and $l$ is the length of half-waves.

$$w_f = A[1 - cos(\frac{2\pi x}{l})] \tag{5.1}$$

The principle of minimum total potential energy is employed to find the critical wrinkling load. The total potential energy $\Pi$ is composed of the strain energy of the elastic foundation $U_c$, the strain energy associated with the bending of the face-sheet $U_f$, and $W$, which is the work done by the compressive load, as following.

$$\Pi = U_f + U_c + W \tag{5.2}$$

The expressions for each components of the total potential of the system is shown in Equation 5.3, 5.4 and 5.5, respectively.

$$U_c = \frac{k}{2}\int_0^l w_f^2 = \frac{3A^2kl}{4} \tag{5.3}$$

$$U_f = \frac{E_f I_f}{2}\int_0^l (\frac{\partial^2 w_f}{\partial x^2})^2 dx = \frac{\pi^4 A^2 E_f {t_f}^3}{3l^3} \tag{5.4}$$

$$W = -\frac{P}{2}\int_0^l (\frac{\partial w_f}{\partial x})^2 dx = -\frac{P\pi^2 A^2}{4l} \tag{5.5}$$

where $E_f$ is the elastic modulus of the face-sheet material, $k$ is the stiffness of the elastic foundation, $I_f = {t_f}^3/12$ is the second moment of area of the face-sheet cross-section and $P$ is the compressive load applied to the face-sheets. The stiffness constant $k$ of the elastic foundation is suggested as $k = 2E_c/t_c$ in [36].

According to the principle of minimum total potential energy, the differentiation of the total potential energy with respect to the A, the non-zero amplitude, is set to zero, and the load expression is found, Equation 5.6.

$$P = \frac{4\pi^4 E_f t_f^3 + 9l^4 k}{12\pi^2 l^2} \tag{5.6}$$

The critical half wave-length, Equation 5.7 is obtained by differentiating Equation 5.6 with respect to $l$. The expression of critical half-wave length is substituted back to Equation 5.6 and the critical stress is found, Equation 5.8.

$$l_{cr} = \frac{\sqrt{6}\pi (E_f t_f^3 k^3)^{\frac{1}{4}}}{3k} \tag{5.7}$$

$$\sigma_{cr} = \sqrt{\frac{2E_f E_c t_f}{t_c}} \tag{5.8}$$

The same method but different deformation function was proposed by Mondal and Nakhla [98].The polynomial deformation function and the corresponding critical stress in their paper are

$$w_f = A[(\frac{x}{l})^2 - 2(\frac{x}{l})^3 + (\frac{x}{l})^4] \tag{5.9}$$

$$\sigma_{cr} = \sqrt{\frac{7E_f E_c t_f}{3t_c}} \tag{5.10}$$

The sinusoidal deformation function is used in [36]. The function is assumed to be

$$w_f = Asin(\frac{x}{l}) \tag{5.11}$$

When the core is simplified as Winkler foundation, the corresponding critical stress (Winkler model) provided in [36] is

$$\sigma_{cr} = \frac{\sqrt{3}}{3}\sqrt{\frac{2E_f E_c t_f}{t_c}} \tag{5.12}$$

Comparing Equation 5.8, 5.10 and 5.12, it can be seen that the differences between the three equations are constant for a given sandwich beam. The critical wrinkling stress proposed in this paper is equal to $\sqrt{3}$ times of that in [36].

## 5.4 Finite element analysis

In this section, the two-dimension finite element analysis is employed using ABAQUS to simulate the wrinkling of sandwich structures under in-plane compressions. The material selections and specimen geometries are extracted from existing testings documented in literature. The FEA results are compared with that of analytical models and testings in literature.

### 5.4.1 Description of the finite element model

In the two-dimension finite element model, the sandwich structure is discretized to face-sheets and core. Four-node bilinear plane stress solid elements are used for the

core. The face-sheet is modeled by either linear beam elements or four-node bilinear plane stress solid elements. The advantage of using beam elements is that the model is simplified and the computation time is therefore reduced, while the drawback induced is that the beam elements are assigned to the nodes in the top and bottom surfaces of the core to connect them to the core solid elements. Consequently, the distance between the centerline of the face-sheet and the interface of core and face-sheets is neglected. Considering the face-sheets thickness is much smaller compared to the core thickness, the error introduced is trivial. In this scenario, the size of the beam element is determined by the longitudinal size of the 2D plane stress solid elements for the core.

When the isotropic material is used for face-sheets, both beam elements and plane stress solid elements can be easily employed. However, for composite laminated face-sheets, the mechanical properties of the laminate should be provided or calculated before modeling it using beam elements. Otherwise, the laminate should be discretized according the stacking sequence of lamina, each layer of which is represented by 2D solid elements.

### 5.4.2 Winkling of sandwich beam consisted of isotropic face-sheets

The materials and geometries of the sandwich beam for the FEA model are from [1]. The 24ST clad aluminum alloy was used as the face-sheet and the Cork was used as the foam material. The sandwich specimens were constructed by bonding the facings to the core by means of a primary and a secondary glue [28]. The details of specimen

geometries and material properties are listed in Table 5.1. The width of the specimen is 2 inches.

Table 5.1: Geometrical parameters and material properties [1]

| **Geometries and properties** | **Values** |
|---|---|
| Total thickness of sandwich beam, H (in) | 1.0392 |
| Width of sandwich beam, B (in) | 2.0 |
| Thickness of facing, $t_f$ (in) | 0.0196 |
| Thickness of core, $t_c$ (in) | 1.0 |
| Length of sandwich, L (in) | 3.63 |
| Elastic modulus of Aluminum facing, $E_f$ (ksi) | 9500 |
| Poisson's ratio of Aluminum facing, $\nu_f$ | 0.25 |
| Elastic modulus of Cork core, $E_c$ (ksi) | 1.18 |
| Poisson's ratio of Cork core, $\nu_c$ | 0.136 |

The convergence of the FEA model is first checked to find the proper element size. The change of critical load with respect to the number of elements used in the mesh is plotted to find the trend. According to the convergence trend, the number of 400 elements in the length direction and the number of 80 elements in the thickness direction for the core are efficient for the simulation. The multi-point constraint boundary conditions at two ends are created to make the end lines behave as a rigid surface. The nodes at the end lines are allowed to move in the thickness direction but are always constrained in the straight line connecting two extreme end nodes of the core. The straight line can be stretched linearly and rotates around its central node.

The translational freedoms of the node at the middle of the left end are constrained. The compressive load in the length direction is applied to the node at the middle of the right end, the thickness direction translational freedom of which is also constrained. The illustration of multi-point constraints and boundary conditions is shown in Figure 5.2. The critical load is then evaluated based on the smallest eigenvalue yielded by ABAQUS and the corresponding wrinkling mode can also be found.

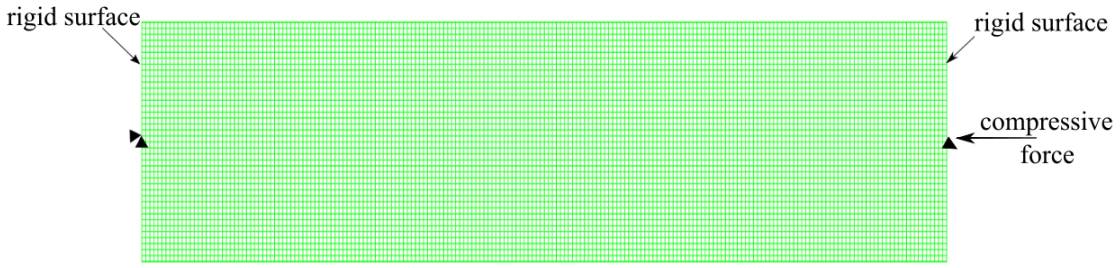


Figure 5.2: Illustration of boundary conditions and load

#### 5.4.2.1 Effect of different boundary conditions

When the multi-point constraints (MPC) are applied at the two ends, the wrinkling mode of the sandwich specimen is shown below, Figure 5.3. In this scenario, the rotational freedoms of the nodes at two ends are not constrained. It can be found that the edge wrinkling phenomenon occurs. Comparing the FEA results with that of testing, Table 5.2, a trivial error is found. This is because the failure mode in the testing was actually edge wrinkling instead of wrinkling, which can be verified by the observing the deformation profiles of the specimen provided in [1].

When the edge winkling modes are ignored, the wrinkling mode corresponding

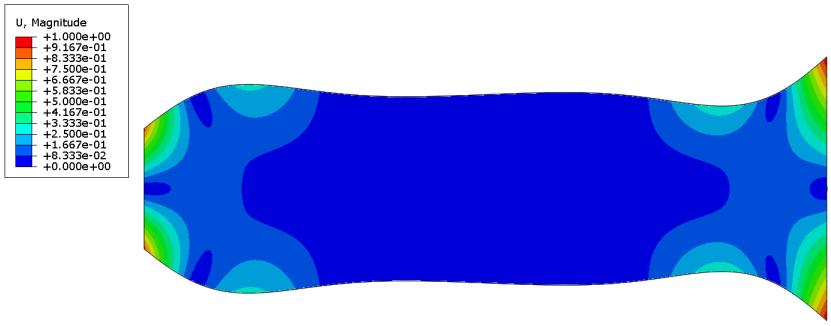


Figure 5.3: Edge Wrinkling (MPC, rotational freedoms of end nodes enabled)

Table 5.2: Comparison between FEA and testing results

| FEA (MPC, rotational freedoms of end nodes enabled) | Testing | Error (%) |
|---|---|---|
| 373.89 lb/in | 385.67 lb/in | 3.05 |

to the lowest compressive load from the same FEA model is shown in Figure 5.4. The compressive load in this situation is 498.84 lb/in. If the rotational freedoms of end nodes is disabled, the critical wrinkling mode is shown in Figure 5.5. The corresponding load is 504.07 lb. The effect of the rotational freedom is illustrated by comparing the two figures. The comparison of different critical loads using MPC is provided in Table 5.3. It shows that when the MPC is applied and the end nodes rotation is allowed, edge wrinkling is critical. The winkling loads with rotational freedoms of end nodes disabled are higher. With the end nodes rotational freedoms enabled, both edge wrinkling and wrinkling can be found.

The critical wrinkling load of the end nodes rotational freedoms enabled situation is then compared with the analytical values in Table 5.4. The polynomial equation represents the model proposed by Modal and Nakhla [98]. It is apparent that the

FEA result is close to that of the classic models (Winkler, Allen, Plantema, Hoff and Mautner, Niu and Talreja), and the present analytical solution and the polynomial equation yield much higher predictions. The reason of the discrepancy will be explained later.

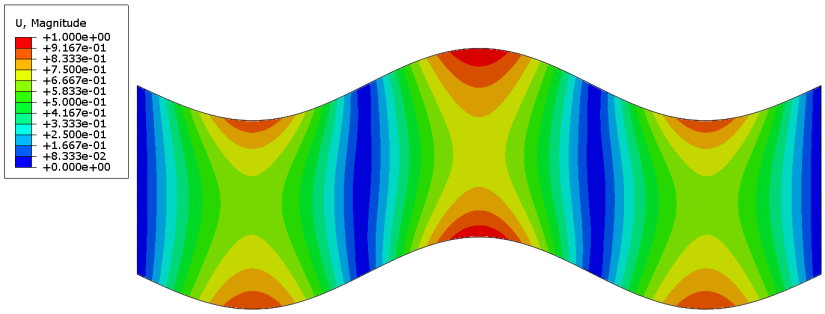


Figure 5.4: Wrinkling mode with MPC (rotation abled)

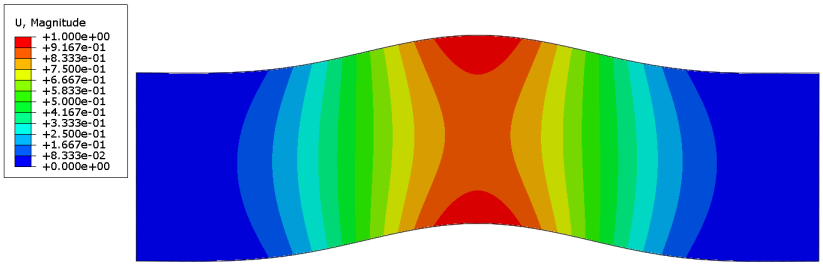


Figure 5.5: Wrinkling mode with MPC (rotation disabled)

#### 5.4.2.2 Effect of face-sheet element types

In this part, two different ways to model the face-sheets of the sandwich beam are compared. The first method is to model the face-sheet using the beam element, as the model in the previous section, while the second one is to use 2D solid elements.

Table 5.3: Comparison of different critical loads using MPC

| Edge wrinkling | Wrinkling (rotation enabled) | Wrinkling (rotation disabled) |
|---|---|---|
| 373.89 lb/in | 498.84 lb/in | 504.07 lb/in |

Table 5.4: Comparison of theoretical and FEA results

| **Method/Model** | **Value (lb/in)** | **Error(%)** |
|---|---|---|
| Present analytical solution | 821.74 | 64.73 |
| Winkler | 474.43 | 4.9 |
| Allen | 553.27 | 10.9 |
| Plantema | 515.32 | 3.3 |
| Hoff and Mautner | 551.70 | 10.60 |
| Niu and Talreja | 566.13 | 13.49 |
| Polynomial equation | 887.58 | 77.93 |

The number of elements in the thickness direction of face-sheets is four when the 2D solid element is chosen.

Similar to the beam element scenario, both edge wrinkling and wrinkling are found when the rotational freedoms of the end nodes are enabled, as shown in Figure 5.6. When the rotational freedoms of the nodes at ends are constrained, the edge wrinkling disappears and the critical wrinkling mode is shown in Figure 5.7.

The results from the FEA model using 2D solid elements for face-sheets are compared with that from testings, and they are found close, Table 5.5. The critical loads are also compared when MPC and 2D solid elements for face-sheets are used, Table

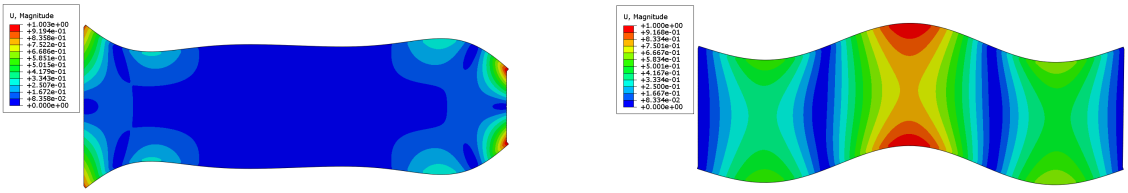

(a) Edge wrinkling (b) Wrinkling

Figure 5.6: Illustration of edge wrinkling and wrinkling (2D solid elements for face-sheet)

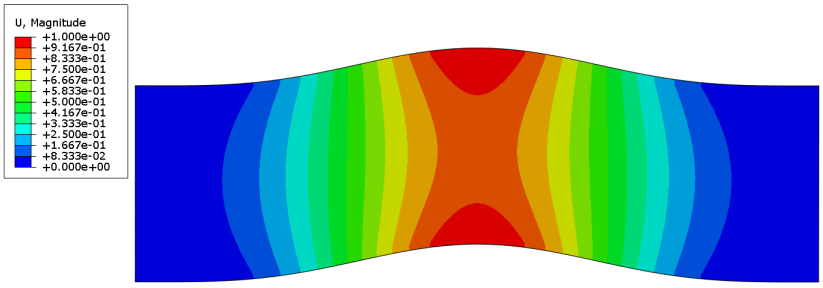


Figure 5.7: Wrinkling mode with MPC (2D solid elements for face-sheet, rotation disabled)

5.6. Taking the value of winkling (rotation enabled) as a reference, the comparison of FEA and analytical results are presented in Table 5.7.

In a summary, the element types of face-sheets have a very small effect on the critical wrinkling load. Whether beam elements or 2D solid elements are used, the effect of boundary conditions is the same and significant. The edge wrinkling is critical for both element types. When the rotational freedoms of the nodes at two ends are disabled, the boundary conditions are actually clamp-clamp, so that the corresponding critical load is the highest. When 2D solid elements are implemented, the FEA result are more accurate because smaller errors are found when they are compared

Table 5.5: Comparison of FEA with testing results (2D solid element for the face-sheets)

| FEA (MPC, rotational freedoms of end nodes enabled) | testing | Error (%) |
|---|---|---|
| 384.38 lb/in | 385.67 lb/in | 0.33 |

Table 5.6: Comparison of different critical loads using MPC (2D solid element for the face-sheets)

| Edge wrinkling | Wrinkling (rotation enabled) | Wrinkling (rotation disabled) |
|---|---|---|
| 384.38 lb/in | 522.89 lb/in | 526.88 lb/in |

with analytical and testing ones. Ignoring the distance between the centerline of skins and interface may be the reason why the beam element is less accurate.

### 5.4.3 Wrinkling of sandwich structure with laminated face-sheets

Besides the sandwich structure with Aluminum face-sheets, sandwich panels with carbon fibre vinylester face-sheets are chosen for the comparison between testing and FEA results. The face-sheet was laminated using four unidirectional layers in the stacking sequence $[0/90]_s$, resulting in a total thickness of approximately 1 mm. The material properties of the lamina are shown in Table 5.8. In the test, carbon fibre laminate tabs of 2mm thick and 25mm wide were bonded to the two ends of the specimen. The specimens were placed between two plates, one of which was fixed and the other was allowed to move to compress the sandwich panel. Divinycell H-

Table 5.7: Comparison of analytical and FEA results (2D solid element for the face-sheets)

| **Method/Model** | **Value (lb/in)** | **Error(%)** |
|---|---|---|
| Present analytical solution | 821.74 | 57.15 |
| Winkler | 474.43 | 9.27 |
| Allen | 553.27 | 5.81 |
| Plantema | 515.32 | 1.45 |
| Hoff and Mautner | 551.70 | 5.51 |
| Niu and Talreja | 566.13 | 8.27 |
| Polynomial equation | 887.58 | 69.75 |

grade foams were used as core materials. The geometrical parameters of the chosen specimen are demonstrated in Table 5.9 [2].

Table 5.8: Material properties of the carbon-vinylester lamina [2]

| **Properties** | **Values** |
|---|---|
| $E_1$ (GPa) | 107 |
| $E_2$ (GPa) | 15 |
| $G_{12}$ (GPa) | 4.3 |
| $\nu_{12}$ | 0.3 |
| $\nu_{21}$ | 0.043 |
| $t_f$ (mm) | 0.25 |

Table 5.9: Geometrical parameters and material properties of the composites sandwich panel

| **Geometries and properties** | **Values** |
|---|---|
| Total thickness of sandwich beam, H (mm) | 52 |
| Thickness of facing, $t_f$ (mm) | 1 |
| Thickness of core, $t_c$ (mm) | 50 |
| Length of sandwich, L (mm) | 200 |
| Elastic modulus of H30, $E_c$ (MPa) | 20 |

The 2D solid elements are used to model the laminate face-sheets. There are four elements in the thickness direction of the face-sheet, and the properties of the lamina are assigned to the four layers of elements according to the laminate stacking sequences. The finite element model resembles the test setups with least simplification. The two tabs bonded in to the specimen in the experiment are also considered in the FEA model. The plates used to compress the specimen in the test are modeled by two rigid surfaces. The wrinkling mode from FEA is shown in Figure 5.8.

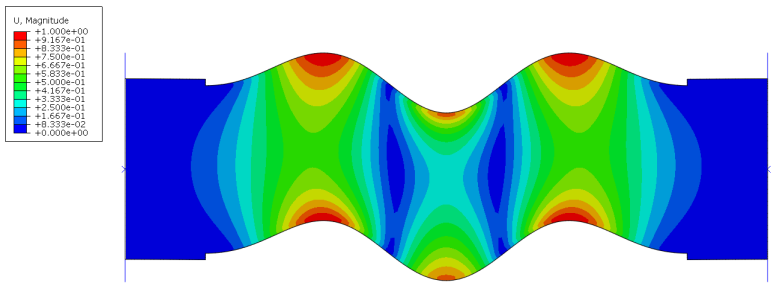


Figure 5.8: Sandwich panel with laminated composites face-sheet

#### 5.4.3.1 Comparison of analytical, FEA and testing results

The FEA result is compared with the testing result, as shown in Table 5.10. It is found that the FEA model over predict the results by 23.94%. The error may come from the simulation or the testings. To figure out the possible reasons for the discrepancies, the FEA result is further compared with analytical ones, as shown in Table 5.11. Except for the Winkler model, all the other models yield high wrinkling loads than the testing result. It is worth to mention that Plantema's model and the model of Hoff and Mautner yield results very close to that of FEA.

Table 5.10: Comparison of FEA with testing results

| FEA | Testing | Error (%) |
|---|---|---|
| 219990 (N/M) | 177500 (N/M) | 23.94 |

Table 5.11: Comparison of analytical with FEA results

| **Method/Model** | **Value (N/M)** | **Error(%)** |
|---|---|---|
| Prisent analytical solution | 221700 | 0.78 |
| Winkler | 128000 | 41.82 |
| Allen | 183150 | 16.75 |
| Plantema | 214070 | 2.69 |
| Hoff and Mautner | 229180 | 4.18 |
| Niu and Talreja | 190180 | 13.55 |
| Polynomial equation | 239470 | 8.85 |

In [2], the Plantema's model was chosen as analytical criteria, and the testing results were lower compared with that from Plantema's model. The FEA model in this paper and Plantema's model have close results. It is safe to conclude that the lower testing result was resulted by the geometrical imperfection of the sandwich panel or other error from testings. Meanwhile, the FEA model is demonstrated to be reliable in predicting the wrinkling load.

In the section 5.4.2, the Winkler model predicts the critical wrinkling load accurately while the analytical solution presented in this paper is much higher. However, in this section, the analytical solution presented in this paper is close to the FEA result while the Winkler model yields much lower prediction. The reason for this discrepancies is that the assumption of Winkler elastic foundation to represent the core material is over-simplified. Winkler Model can only accurately predict the wrinkling load for sandwich structure of specific face-sheet to core thickness ratios, as demonstrated in a plot in [36]. As mentioned earlier, the critical wrinkling stress proposed in this paper is equal to $\sqrt{3}$ times of that in [36], which means the present analytical solution has the same limitation as the Winkler model.

## 5.5 Discussion and conclusion

The analytical solution and finite element analysis are applied to investigate the wrinkling of sandwich structure. A new deformation function is proposed for the wrinkling shape of face-sheets and corresponding critical wrinkling load is derived. In the finite element simulation, the effect of boundary conditions and the element types of face-sheets are considered and compared. For the finite element analysis, the face-

sheets of sandwich structures could be isotropic material or laminated composites. The proposed analytical solution and FEA results are compared with that of testings and other classic analytical models.

It is found that the analytical solution presented in the paper cannot always accurately predict the critical load. The accuracy is dependent of the geometries of sandwich structures. The application of the Winkler elastic foundation to represent the core is the reason for the limitation. For FEA, the rotational freedoms of end nodes are significant in achieving accurate simulations. When the ends are allowed to rotate freely, edge wrinkling is critical for that specimen. In the same model, critical wrinkling loads can be found when the edge wrinkling is skipped. The wrinkling can also be obtained by constraining the rotations of the two ends of the sandwich structure. The FEA results are close to that from Allen's, Plantema's, Hoff and Mautner's, and Niu and Talreja's models. Both beam and 2D elements are acceptable to model face-sheets, yet 2D elements give more accurate results.

For the sandwich panel with laminated composites face-sheets, the FEA model resembles the actual testing setups and the specimen used. Although the FEA result is higher compared to the testing one, it is verified by the other well-known analytical models. The lower testing load comes from the geometric imperfections of the sandwich structure or other sources of errors during the testing.

# Chapter 6

# Conclusions

This section is divided into two parts. The first part reviews the problems solved in the three papers and summarizes the methods and theories. The second part proposes possible future work based on the research finished in the papers.

## 6.1 Summary

The thesis accomplished the feasibility study of composites sandwich structure, web-core sandwich structure especially, for large ship structure. The cost estimation method for composites structure manufacturing was proposed. The buckling phenomenon of web-core sandwich structures was studied. The finite element analysis simulation was implemented to facilitate the sandwich structure wrinkling research .

### 6.1.1 Cost estimation of web-core sandwich structure manufacturing

The vacuum assisted resin transfer molding (VARTM) method was selected for the manufacturing of large web-core sandwich structure. The specific process steps were presented. The method and framework in [6, 13, 14] were used and extended in the thesis. Due to the lack of 'first order dynamic model' constants for the resin infusion time estimation, a method to estimate VRATM resin infiltration based on resin transfer molding (RTM) was used to solve the problem. The manufacturing cost, structure strength and stiffness were compared between the web-core composites sandwich hatch cover and conventional steel hatch cover. The potentials of using composites sandwich structures were revealed.

### 6.1.2 Buckling web-core sandwich structure

Different from the buckling of conventional sandwich beam or plate, the buckling wave shape of web-core sandwich structures is usually non-sinusoidal because of the effect of the web. The web was simplified as simply supported or clamped end in some research such as [53, 71]. In the thesis, the web was represented as rotational spring end and the core was represented as the Pasternak foundation. The variational iteration method (VIM) was used to investigate the effects of web and core on the critical buckling load. The approximation results from VIM was verified by the exact results. The VIM was then used in the practical web-core ship structure and design suggestion was provided.

### 6.1.3 Finite element simulation for the wrinkling of sandwich structure

Finite element simulation was implemented in the prediction of sandwich structure wrinkling. The sandwich structures with both isotropic and composites face-sheets were covered in the thesis. The effects of different boundary conditions were studied. The finite element analysis simulation results were compared with both existing testing and theoretical results.

## 6.2 Future work

Mathematical models for the estimation of fabrication time of web-core sandwich structure were presented in Chapter 3. The estimated time has not been validated by experiments. As an extension of the work in Chapter 3, experiments to measure the time of each fabrication step are needed. Further more, the web-core sandwich structure built in the time measurement experiments can be used as specimen for mechanical performance tests.

In Chapter 4, the two Pasternak parameters were cited from the work of [53]. The two parameters were modified based on the finite element analysis simulation results. Different expressions for the Pasternak foundation parameters can be found in literature. Therefore, special attention should be paid to choose the proper expressions. Besides, more rigorous derivations of the parameter expressions are of significant, especially when the wrinkling shape is non-sinusoidal. Moreover, finite element analysis simulation can be carried out to validate the analytical solutions in the chapter.

For the finite element analysis simulation of sandwich structure wrinkling, the effects of boundary conditions and face-sheets elements were investigated in Chapter 5. Compared to the whole structure model, another method, the periodic model, was used in the literature [41, 43]. It will be interesting to compare the methods and their results. The available testing results regarding sandwich wrinkling are limited. Disparities are commonly found between theoretical and testing results. More sophisticated testings are expected to be carried out.

To conclude, the wrinkling phenomenon is still an essential consideration in the design of sandwich structure. The development of complex sandwich structure makes it more difficult to predict the wrinkling failure. More efforts are needed for the new theoretical modeling, advanced finite element analysis simulation and testing with innovative devices and technologies.

# Bibliography

[1] American Mathematical Society and University of Michigan. *Elasticity. [Proceedings of the 3rd symposium in applied mathematics of the American Mathematical Society held at the University of Michigan, June 14-16, 1949]*. McGraw-Hill, New York, 1950.

[2] Linus Fagerberg. Wrinkling and compression failure transition in sandwich panels. *Journal of Sandwich structures and materials*, 6(2):129–144, 2004.

[3] M DOttavio and O Polit. Linearized global and local buckling analysis of sandwich struts with a refined quasi-3d model. *Acta Mechanica*, 226(1):81–101, 2015.

[4] Robert J Scott and John H Sommella. Feasibility study of glass reinforced plastic cargo ship. Technical report, DTIC Document, 1971.

[5] MJ Robinson and JB Kosmatka. Light-weight fiber-reinforced polymer composite deck panels for extreme applications. *Journal of Composites for Construction*, 12(3):344–354, 2008.

[6] Sascha Marcel Haffner. *Cost modeling and design for manufacturing guidelines for advanced composite fabrication*. PhD thesis, Massachusetts Institute of Technology, 2002.

[7] Eric Greene. Design guide for marine applications of composites. *NTIS(USA)*, page 350, 1997.

[8] AP Mouritz, E Gellert, P Burchill, and K Challis. Review of advanced composite structures for naval ships and submarines. *Composite structures*, 53(1):21–42, 2001.

[9] SAND CORE. Best practise guide for sandwich structures in marine application. *NewRail: University of Newcastle*, 2005.

[10] Pentti Kujala and Alan Klanac. Steel sandwich panels in marine applications. *Brodogradnja*, 56(4):305–314, 2005.

[11] China Classification Society. Guidelines for the application of steel sandwich panel construction to ship structure. *CSS Rules for Classification of Sea-going Steel Ships*, 2007.

[12] J Lorenzana, A Kokawa, T Bettner, F Timson, J Proctor, HJ Behrens, L Lyle, M Woo, and L Bernhardt. Advanced composite cost estimating manual. Technical report, Technical Report AFFDL-TR-76-87, Northrop Grumman Corporation, Aircraft Division, Hawthorne, California, USA, 1976.

[13] Timothy Gutowski, David Hoult, Greg Dillon, Ein-Teck Neoh, Stuart Muter, Eric Kim, and Mawuli Tse. Development of a theoretical cost model for advanced composite fabrication. *Composites Manufacturing*, 5(4):231–239, 1994.

[14] Ein-Teck Neo. *Adaptive framework for estimating fabrication time.* PhD thesis, Massachusetts Institute of Technology, 1995.

[15] Jinrui Ye, Boming Zhang, and Haiming Qi. Cost estimates to guide manufacturing of composite waved beam. *Materials & Design*, 30(3):452–458, 2009.

[16] Christos Kassapoglou. Minimum cost and weight design of fuselage frames: Part a: design constraints and manufacturing process characteristics. *Composites Part A: Applied Science and Manufacturing*, 30(7):887–894, 1999.

[17] K Wang, D Kelly, and S Dutton. Multi-objective optimisation of composite aerospace structures. *Composite Structures*, 57(1):141–148, 2002.

[18] N Bernet, MD Wakeman, P-E Bourban, and J-AE Månson. An integrated cost and consolidation model for commingled yarn based composites. *Composites Part A: applied science and manufacturing*, 33(4):495–506, 2002.

[19] Markus Kaufmann, Dan Zenkert, and Christophe Mattei. Cost optimization of composite aircraft structures including variable laminate qualities. *Composites Science and Technology*, 68(13):2748–2754, 2008.

[20] Nand K Jha. Probabilistic cost estimation in advance of production in a computerized manufacturing system through stochastic geometric programming. *Computers & industrial engineering*, 30(4):809–821, 1996.

[21] H Jahan-Shahi, E Shayan, and S Masood. Cost estimation in flat plate processing using fuzzy sets. *Computers & industrial engineering*, 37(1):485–488, 1999.

[22] E Shehab and H Abdalla. An intelligent knowledge-based system for product cost modelling. *The international journal of advanced manufacturing technology*, 19(1):49–65, 2002.

[23] Mark Eklin, Yohanan Arzi, and Avraham Shtub. Model for cost estimation in a finite-capacity stochastic environment based on shop floor optimization combined with simulation. *European journal of operational research*, 194(1):294–306, 2009.

[24] GS Gough, CF Elam, and NA De Bruyne. The stabilization of a thin sheet by a continuous supporting medium. *JR Aeronaut. Soc*, 44(349):12–43, 1940.

[25] NJ Hoff and Mautner SE. The buckling of sandwich-type panels. *Journal of the Aeronautical Sciences (Institute of the Aeronautical Sciences)*, 12(3), 1945.

[26] Stephen P Timoshenko and James M Gere. Theory of elastic stability. 1961. *McGrawHill-Kogakusha Ltd, Tokyo*, 1961.

[27] SV Nardo. An exact solution for the buckling load of flat sandwich panels with loaded edges clamped. *Journal of the Aeronautical Sciences (Institute of the Aeronautical Sciences)*, 20(9), 1953.

[28] Charles B Norris, Wilhelm S Ericksen, HW March, CB Smith, Kenneth H Boller, et al. Wrinkling of the facings of sandwich construction subjected to edgewise compression. *Series: FPL Reports (Historical)*, 1961.

[29] Frederik J Plantema. Sandwich construction, 1966.

[30] Arthur Searle Benson and J Mayers. General instability and face wrinkling of sandwich plates-unified theory and applications. *AIAA journal*, 5(4):729–739, 1967.

[31] Howard G Allen. *Analysis and Design of Structural Sandwich Panels: The Commonwealth and International Library: Structures and Solid Body Mechanics Division*. Elsevier, 1969.

[32] Michael A Stiftinger and Franz G Rammerstorfer. Face layer wrinkling in sandwich shellstheoretical and experimental investigations. *Thin-Walled Structures*, 29(1):113–127, 1997.

[33] Kangmin Niu and Ramesh Talreja. Modeling of wrinkling in sandwich panels under compression. *Journal of Engineering Mechanics*, 125(8):875–883, 1999.

[34] BK Hadi and FL Matthews. Development of benson–mayers theory on the wrinkling of anisotropic sandwich panels. *Composite structures*, 49(4):425–434, 2000.

[35] Wooseok Ji and Anthony M Waas. Global and local buckling of a sandwich beam. *Journal of engineering mechanics*, 2007.

[36] Leif A Carlsson and George A Kardomateas. *Structural and failure mechanics of sandwich composites*, volume 121. Springer Science & Business Media, 2011.

[37] TRA Pearce and JPH Webber. Experimental buckling loads of sandwich panels with carbon fibre faceplates. *Aeronautical Quarterly*, 24:295–312, 1973.

[38] Kyriakides S Webber JPH and Lee CT. On the wrinkling of anisotropic sandwich column with laminated cross-ply faces. *Aeronaut Quart*, page 264272, 1976.

[39] NA Fleck and I Sridhar. End compression of sandwich columns. *Composites Part A: applied science and manufacturing*, 33(3):353–359, 2002.

[40] EE Gdoutos, IM Daniel, and K-A Wang. Compression facing wrinkling of composite sandwich structures. *Mechanics of materials*, 35(3):511–522, 2003.

[41] Walter K Vonach and Franz G Rammerstorfer. Wrinkling of thick orthotropic sandwich plates under general loading conditions. *Archive of Applied Mechanics*, 70(5):338–348, 2000.

[42] BK Hadi. Wrinkling of sandwich column: comparison between finite element analysis and analytical solutions. *Composite Structures*, 53(4):477–482, 2001.

[43] Linus Fagerberg and Dan Zenkert. Imperfection-induced wrinkling material failure in sandwich panels. *Journal of Sandwich Structures and Materials*, 7(3):195–219, 2005.

[44] Milton O Critchfield, Thomas D Judy, and Alan D Kurzweil. Low-cost design and fabrication of composite ship structures. *Marine structures*, 7(2):475–494, 1994.

[45] LB Nquyen, Thomas Juska, and SJ Mayes. Evaluation of low cost manufacturing technologies for large scale composite ship structures. In *Proceedings of the 38th Structures, Structural Dynamics and Materials Conference, Kissimmee, FL*, pages 7–10, 1997.

[46] Konstantinos Galanis. *Hull Construction with Composite Materials for Ships over 100 m in length*. PhD thesis, Massachusetts Institute of Technology, 2002.

[47] NC Correia, F Robitaille, AC Long, CD Rudd, P Simacek, and Suresh G Advani. Use of resin transfer molding simulation to predict flow, saturation, and

compaction in the vartm process. *Journal of fluids engineering*, 126(2):210–215, 2004.

[48] KT Hsiao, R Mathur, SG Advani, JW Gillespie, and BK Fink. A closed form solution for flow during the vacuum assisted resin transfer molding process. *Journal of manufacturing science and engineering*, 122(3):463–475, 2000.

[49] NC Correia, F Robitaille, AC Long, CD Rudd, P Šimáček, and SG Advani. Analysis of the vacuum infusion moulding process: I. analytical formulation. *Composites Part A: Applied Science and Manufacturing*, 36(12):1645–1656, 2005.

[50] Chensong Jonathan Dong. Development of a process model for the vacuum assisted resin transfer molding simulation by the response surface method. *Composites Part A: Applied Science and Manufacturing*, 37(9):1316–1324, 2006.

[51] Chensong Jonathan Dong. An equivalent medium method for the vacuum assisted resin transfer molding process simulation. *Journal of composite materials*, 40(13):1193–1213, 2006.

[52] R Wang and K Ravi-Chandar. Mechanical response of a metallic aortic stentpart ii: a beam-on-elastic foundation model. *Journal of applied mechanics*, 71(5):706–712, 2004.

[53] Hans Kolsters and Dan Zenkert. Buckling of laser-welded sandwich panels. part 2: Elastic buckling normal to the webs. *Proceedings of the Institution of Mechanical Engineers, Part M: Journal of Engineering for the Maritime Environment*, 220(2):81–94, 2006.

[54] Jialai Wang and Chao Zhang. Three-parameter, elastic foundation model for analysis of adhesively bonded joints. *International Journal of Adhesion and Adhesives*, 29(5):495–502, 2009.

[55] SC Pradhan and GK Reddy. Buckling analysis of single walled carbon nanotube on winkler foundation using nonlocal elasticity theory and dtm. *Computational Materials Science*, 50(3):1052–1056, 2011.

[56] Theodor Von Karman and Maurice A Biot. *Mathematical methods in engineering*. McGraw-Hill, 1940.

[57] CM Wang and Chang Yi Wang. *Exact solutions for buckling of structural members*, volume 6. CRC press, 2004.

[58] Emil Winkler. *Die lehre von der elasticitaet und festigkeit*. 1868.

[59] Miklós Hetényi. *Beams on elastic foundation: theory with applications in the fields of civil and mechanical engineering*. University of Michigan, 1946.

[60] PL Pasternak. On a new method of analysis of an elastic foundation by means of two foundation constants. *Gosudarstvennoe Izdatelstvo Literaturi po Stroitelstvu i Arkhitekture, Moscow*, 1954.

[61] Arnold D Kerr. Elastic and viscoelastic foundation models. *Journal of Applied Mechanics*, 31(3):491–498, 1964.

[62] Arnold D Kerr. A study of a new foundation model. *Acta Mechanica*, 1:135–147, 1965.

[63] C Sundararajan. Stability of columns on elastic foundations subjected to conservative and non-conservative forces. *Journal of Sound and Vibration*, 37(1):79–85, 1974.

[64] T Yokoyama. Vibration analysis of timoshenko beam-columns on two-parameter elastic foundations. *Computers & structures*, 61(6):995–1007, 1996.

[65] K Morfidis and IE Avramidis. Generalized beam-column finite element on two-parameter elastic foundation. *Structural Engineering and Mechanics*, 21(5):519–537, 2005.

[66] AN Kounadis, J Mallis, and A Sbarounis. Postbuckling analysis of columns resting on an elastic foundation. *Archive of Applied Mechanics*, 75(6-7):395–404, 2006.

[67] Feng Zhaohua and Robert D Cook. Beam elements on two-parameter elastic foundations. *Journal of Engineering Mechanics*, 109(6):1390–1402, 1983.

[68] Robert Levy. Buckling optimization of beams and plates on elastic foundation. *Journal of engineering mechanics*, 116(1):18–34, 1990.

[69] Y Xiang, S Kitipornchai, and KM Liew. Buckling and vibration of thick laminates on pasternak foundations. *Journal of engineering mechanics*, 122(1):54–63, 1996.

[70] KY Lam, CM Wang, and XQ He. Canonical exact solutions for levy-plates on two-parameter foundation using green's functions. *Engineering structures*, 22(4):364–378, 2000.

[71] Sontipee Aimmanee and Jack R Vinson. Analysis and optimization of foam-reinforced web core composite sandwich panels under in-plane compressive loads. *Journal of Sandwich Structures and Materials*, 4(2):115–139, 2002.

[72] LH Yu and CY Wang. Buckling of rectangular plates on an elastic foundation using the levy method. *AIAA journal*, 46(12):3163–3167, 2008.

[73] Dimitrios S Sophianopoulos and Konstantinos S Papachristou. In-plane stability of uniform steel beam-columns on a pasternak foundation with zero end-shortening. *Archive of Applied Mechanics*, 82(10-11):1653–1662, 2012.

[74] L Sironic, NW Murray, and RH Grzebieta. Buckling of wide struts/plates resting on isotropic foundations. *Thin-walled structures*, 35(3):153–166, 1999.

[75] Casey R Briscoe, Susan C Mantell, and Jane H Davidson. Shear buckling in foam-filled web core sandwich panels using a pasternak foundation model. *Thin-Walled Structures*, 48(6):460–468, 2010.

[76] Seval Pinarbasi. Buckling analysis of nonuniform columns with elastic end restraints. *Journal of Mechanics of Materials and Structures*, 7(5):485–507, 2012.

[77] Ji-Huan He. Variational iteration method–a kind of non-linear analytical technique: some examples. *International journal of non-linear mechanics*, 34(4):699–708, 1999.

[78] Ji-Huan He, Guo-Cheng Wu, and F Austin. The variational iteration method which should be followed. *Nonlinear Science Letters A-Mathematics, Physics and Mechanics*, 1(1):1–30, 2010.

[79] Mehmet Tarık Atay and Safa Bozkurt Coşkun. Elastic stability of euler columns with a continuous elastic restraint using variational iteration method. *Computers & Mathematics with Applications*, 58(11):2528–2534, 2009.

[80] George J Simitses and JW Hutchinson. An introduction to the elastic stability of structures. *Journal of Applied Mechanics*, 43:383, 1976.

[81] John Michael Davies. *Lightweight sandwich construction*. John Wiley & Sons, 2008.

[82] Maciej Taczała and Waldemar Banasiak. Buckling of i-core sandwich panels. *Journal of Theoretical and Applied Mechanics*, 42(2):335–348, 2004.

[83] J Romanoff, A Laakso, and P Varsta. Improving the shear properties of web-core sandwich structures using filling material. *Analysis and Design of Marine Structures, Leiden, NL, CRC Press*, pages 133–138, 2009.

[84] D Frank, J Romanoff, and H Remes. Fatigue life improvement of laser-welded web-core steel sandwich panels using filling materials. *Analysis and Design of Marine Structures V*, page 261, 2015.

[85] Eugene E Lundquist and Elbridge Z Stowell. *Critical compressive stress for flat rectangular plates supported along all edges and elastically restrained against rotation along the unloaded edges*. National Advisory Committee for Aeronautics, 1942.

[86] Friedrich Bleich. *Buckling strength of metal structures*. McGraw-Hill, 1952.

[87] Pizhong Qiao and Guiping Zou. Local buckling of elastically restrained fiber-reinforced plastic plates and its application to box sections. *Journal of engineering mechanics*, 128(12):1324–1330, 2002.

[88] Pizhong Qiao and Luyang Shan. Explicit local buckling analysis and design of fiber–reinforced plastic composite structural shapes. *Composite Structures*, 70(4):468–483, 2005.

[89] Pizhong Qiao and Guiping Zou. Local buckling of composite fiber-reinforced plastic wide-flange sections. *Journal of Structural Engineering*, 129(1):125–129, 2003.

[90] László P Kollár. Buckling of unidirectionally loaded composite plates with one free and one rotationally restrained unloaded edge. *Journal of Structural Engineering*, 128(9):1202–1211, 2002.

[91] László P Kollár. Local buckling of fiber reinforced plastic composite structural members with open and closed cross sections. *Journal of Structural Engineering*, 129(11):1503–1513, 2003.

[92] Lawrence C Bank. *Composites for construction: structural design with FRP materials*. John Wiley & Sons, 2006.

[93] Jani Romanoff, Petri Varsta, and Heikki Remes. Laser-welded web-core sandwich plates under patch loading. *Marine structures*, 20(1):25–48, 2007.

[94] Eliseu Lucena Neto, Francisco Alex Correia Monteiro, and Flávio Luiz de Silva Bussamra. Buckling of euler-bernoulli beams with general boundary conditions. 2009.

[95] Jack R Vinson. *Plate and panel structures of isotropic, composite and piezoelectric materials, including sandwich construction*, volume 120. Springer Science & Business Media, 2006.

[96] Arnold D Kerr. On the determination of foundation model parameters. *Journal of Geotechnical Engineering*, 111(11):1334–1340, 1985.

[97] Casey R Briscoe. *Design of lightweight web core sandwich panels and application to residential roofs.* PhD thesis, UNIVERSITY OF MINNESOTA, 2010.

[98] S Mondal and S Nakhla. Simplified failure mode maps for the design of sandwich beams. 2016. Manuscript submitted for publication.